Journal of Catalysis 282 (2011) 128–144

Contents lists available at ScienceDirect

Journal of Catalysis

journal homepage: www.elsevier.com/locate/jcat

Catalytic behaviour of hybrid LNT/SCR systems: Reactivity and in situ FTIR study

L. Castoldi [a], R. Bonzi [a], L. Lietti [a], P. Forzatti [a,*], S. Morandi [b], G. Ghiotti [b], S. Dzwigaj [c]

[a] Dipartimento di Energia, Laboratory of Catalysis and Catalytic Processes and NEMAS, Centre of Excellence, Politecnico di Milano, p.zza L. da Vinci 32, Milano, Italy
[b] Dipartimento di Chimica IFM and NIS, Centre of Excellence, Università di Torino, via P. Giuria 7, Torino, Italy
[c] CNRS, UMR 7197, Laboratoire de Réactivité de Surface, Université Pierre et Marie Curie, 4 place Jussieu, Paris Cedex 05, France

ARTICLE INFO

Article history:
Received 8 April 2011
Revised 1 June 2011
Accepted 2 June 2011
Available online 19 July 2011

Keywords:
LNT
SCR
Pt–Ba/Al_2O_3
Fe-ZSM-5
Hybrid LNT/SCR systems
LNT/SCR dual bed
LNT/SCR physical mixture

ABSTRACT

The NO_x storage-reduction over the single Pt–Ba/Al_2O_3 and Fe-ZSM-5 systems and over the hybrid Pt–Ba/Al_2O_3 + Fe-ZSM-5 systems, both physically mixed and in dual bed configuration with the SCR catalyst placed downstream of the LNT catalyst, is systematically investigated by Isothermal Step Concentration (ISC) experiments and FTIR spectroscopy. The study is accomplished using H_2 as the reductant, in the presence and absence of CO_2 and H_2O and in a wide temperature interval (150–350 °C). The results are explained at the quantitative level by applying a scheme of the reduction of stored NO_x, which implies at first the reduction of nitrates to give NH_3, followed by the reaction of ammonia with NO_x stored downstream in the reactor to give N_2. The following main points have been clarified: (1) the storage of NO_x occurs primarily onto Pt–Ba/Al_2O_3 and is lower in the presence of CO_2 and H_2O because $BaCO_3$ is formed which retards NO_x adsorption; (2) NH_3 formed as intermediate in the reduction of stored NO_x is trapped onto the Fe-ZSM-5 catalyst. The trapping of NH_3 is most favoured when the particles of Pt–Ba/Al_2O_3 and of Fe-ZSM-5 are extensively in contact, as in the LNT/SCR physical mixture, and at low temperature. NH_3 trapped onto Fe-ZSM-5 reacts during the subsequent lean phase with gaseous NO_x slipped from the Pt–Ba/Al_2O_3 particles to give N_2 via SCR; (3) the NO_x removal efficiency is always higher for both LNT/SCR dual bed and physical mixture compared to single LNT, due to the additional contribution of SCR over Fe-ZSM-5 during the lean phase; (4) in the case of the LNT/SCR physical mixture, NH_3 trapped onto the Fe-ZSM-5 particles can be oxidised over the LNT particles upon admission of oxygen to give N_2, N_2O and NO. The selectivity to nitrogen is almost complete at any temperature in the presence of CO_2 and H_2O, while in the absence of CO_2 and H_2O, it increases significantly with temperature and is almost complete at 350 °C; (5) the ammonia slip is low to the best over the LNT/SCR dual bed at any temperature in the absence of CO_2 + H_2O. In the presence of CO_2 and H_2O, the ammonia slip is nil at any temperature over the LNT/SCR dual bed.

© 2011 Elsevier Inc. All rights reserved.

1. Introduction

The improvement in fuel economy and the reduction in the emissions of CO_2 have motivated extensive use of diesel and lean burn gasoline vehicles in recent years. While compliance with previous NO_x regulations (e.g. Euro 5) has been largely achieved so far without resort to NO_x after-treatment, either Selective Catalytic Reduction (SCR) or Nitrogen Storage Reduction (NSR), also quoted as Lean NO_x Trap (LNT) [1–7], will need to be applied to meet the upcoming stringent NO_x emission standards [8,9]. Indeed, the proven technologies of automotive catalysis, the Diesel Oxidation Catalyst (DOC) and the Three Way Catalyst (TWC) used for stoichiometric gasoline engines are not capable to reduce NO_x under net oxidising conditions.

The SCR approach is based on the reaction between NO and NH_3, which is produced by hydrolysis of an aqueous urea solution injected into the exhausts from an on-board tank, according to the standard SCR reaction:

$$4NO + 4NH_3 + O_2 \rightarrow 4N_2 + 6H_2O \quad (1)$$

The activity at low temperature, where most of NO_x emissions are produced, can be improved by positioning a DOC unit upstream of the SCR converter to oxidise NO to NO_2. This allows the occurrence of the fast SCR reaction (2), which is considerably faster than reaction (1) at low temperatures [10,11]:

$$NO + NO_2 + 2NH_3 \rightarrow 2N_2 + 3H_2O \quad (2)$$

Recently, high NO_x removal at low temperature, similar to that of fast SCR, has been reported for the new enhanced SCR reaction [12,13] where nitrate species are injected into the exhausts to boost the NH_3 SCR activity at low temperature without the necessity to pre-oxidising NO as exemplified by:

* Corresponding author. Fax: +39 02 7063 8173.
E-mail address: pio.forzatti@polimi.it (P. Forzatti).

0021-9517/$ - see front matter © 2011 Elsevier Inc. All rights reserved.
doi:10.1016/j.jcat.2011.06.002

$$2NH_3 + 2NO + NH_4NO_3 \rightarrow 3N_2 + 5H_2O \quad (3)$$

Nowadays, metal-substituted zeolites [7], e.g., Fe- or Cu-ZSM-5, may be preferred to traditional vanadia–tungsta–titania catalysts [3,14] in view of their better high-temperature durability, since the SCR catalyst will receive hot gases during regeneration of the upstream DPF.

The LNT system comprises long lean phases in which NO_x emitted in the exhaust gases are adsorbed on the catalyst and subsequent short rich periods of few seconds in which the stored NO_x are reduced by H_2, CO and Hydrocarbons (HC) to produce nitrogen [5,6]. LNT catalysts contain a high surface area support (such as γ-Al_2O_3), an alkaline/alkaline-earth metal oxide (such as BaO) and precious metals (such as Pt).

It has been demonstrated that the storage of NO/O_2 proceeds according to two different pathways [15,16]. The most effective pathway at low temperature, i.e., $T \leqslant 250$ °C, is the 'nitrite route', which consists in the stepwise oxidation of NO at a Pt site followed by adsorption on a neighbouring Ba site to form adsorbed nitrites; these species are then oxidised to nitrates, if the temperature is high enough (i.e. $\geqslant$200 °C). In parallel to the 'nitrite route', oxidation of NO to NO_2 at Pt also occurs and NO_2 can be stored on Ba sites via NO_2 disproportion to give nitrates and gas phase NO ('nitrate route'); this route is active at high temperature ($T \geqslant 250$ °C). Accordingly, stored NO_x are primarily present in the form of nitrates at high temperature.

Concerning the regeneration of the LNT under nearly isothermal conditions (i.e. without release of NO_x in the gas phase), it has been demonstrated that the reduction by H_2 of stored NO_x occurs through the following consecutive reaction scheme [17–22]:

$$Ba(NO_3)_2 + 8H_2 \rightarrow 2NH_3 + BaO + 5H_2O \quad (4)$$

$$3Ba(NO_3)_2 + 10NH_3 \rightarrow 8N_2 + 3BaO + 15H_2O \quad (5)$$

This scheme implies at first the reaction of stored NO_x with H_2 to give NH_3, followed by the reaction of ammonia with NO_x ad-species located downstream in the reactor to give N_2. Besides, it has been shown that reaction (5) is slower that reaction (4), so that it represents the rate determining step in the reduction of stored NO_x.

A third approach to diesel NO_x control is the use of hybrid LNT/SCR configurations. Here, ammonia slipped from the LTN catalyst during the rich phase is adsorbed onto the SCR catalyst bed placed downstream and reacts according to SCR reactions with NO_x present in the exhausts, which have not been trapped onto the NSR catalyst bed during the subsequent lean phase. Accordingly, over the hybrid LNT/SCR system, the NO_x removal efficiency is increased, the ammonia slip is reduced and the PMG usage is lower. This catalytic technology was introduced recently in the US and in Europe by Daimler AG [23].

Several groups have studied the hybrid catalytic system composed of LNT and SCR catalysts from either a technological point of view [24–28] or a fundamental viewpoint [29–32] and have confirmed that the resulting after-treatment devices ensure better NO_x removal and lower ammonia slip compared with the LNT only technology. In most of these studies, NSR experiments have been performed by alternating long lean phases with short rich periods characterised by high concentration of the reductant. Accordingly, relevant temperature effects together with thermal release of NO_x in the gas phase occurred. In view of this, only a qualitative analysis of the data has been generally attempted.

In a previous paper by some of us [33], a preliminary study of hybrid LNT/SCR systems has been performed. Different configurations were investigated, and the NSR cycle was accomplished with small concentration of hydrogen in the rich period and with a He purge in between the lean and the rich phases to prevent thermal release of NO_x and transients in the oxygen concentration upon the lean-fuel rich switch. The experiments have been carried out at the single temperature level of 200 °C, in the absence of CO_2 and H_2O, and a comparison has been given at the quantitative level assuming the in series two steps pathway for the reduction in stored NO_x described by reactions (4) and (5).

In the present paper, a more systematic and complete investigation of the hybrid arrangements with the LNT catalyst placed in front of the SCR catalyst and of the physical mixture of LNT and SCR catalysts (indicated in the following as LNT/SCR double bed and LNT/SCR physical mixture, respectively) is presented, which combines reactivity measurements and in situ FTIR spectroscopy to analyse the species formed in the gas phase and at the catalyst surface during the lean–rich cycles, covers a wide range of temperature (150–350 °C) and also considers the presence of H_2O and CO_2 in the exhausts. As in the previous papers [29,33], the experiments are performed under nearly isothermal conditions (Isothermal Step Concentration experiments, ISC) with small concentration of H_2 to prevent thermal release of stored NO_x so that the chemistry of Pt-catalysed NO_x/H_2 and NO_x/NH_3 could be neglected in the kinetic scheme of the reduction of stored NO_x. The analytical set up allowed for direct analysis of all reaction products, including N_2, N_2O, NO, NO_2, and NH_3; this is specifically required to check the closure of nitrogen balance and in particular to evaluate the amount of nitrogen formed during the lean and rich phases.

Finally, in the present study, in situ FTIR spectroscopy has been used as complementary technique to analyse the species formed at the catalyst surface during the lean–rich cycles.

2. Experimental

2.1. Catalyst preparation and characterisation

A homemade Pt–Ba/Al_2O_3 (1/20/100 w/w) catalyst has been used in this study. As reported elsewhere [15,18] and in accordance with Toyota patents [34], a commercial γ-alumina sample (Versal 250 from UOP) has been impregnated with aqueous solutions of dinitro-diamine platinum (Strem Chemicals, 5% Pt in ammonium hydroxide) and subsequently of barium acetate (Sigma Aldrich, 99%), dried at 80 °C and calcined in air at 500 °C for 5 h after each impregnation step.

The SCR catalyst is a Fe-ZSM-5 sample purchased from Zeolyst International (Fe loading near 1%, w/w, SiO_2/Al_2O_3 molar ratio 23.3), which has been calcined in air at 500 °C for 5 h before use.

Both the LNT and SCR catalysts have been characterised by XRD, surface area and pore size distribution measurements. XRD diffraction spectra have been recorded with a Philips PW 1050/70 diffractometer equipped with a vertical goniometer using a Ni-filtered Cu*K*-α radiation. Surface area and pore size distribution have been determined by N_2 adsorption–desorption at −196 °C with the BET method using a Micromeritics TriStar 3000 instrument. In addition, the Pt dispersion in the LNT catalyst has been estimated by hydrogen chemisorption at 0 °C, upon reduction in H_2 at 300 °C, using a TPD/R/O 1100 Thermo Fischer Instrument and the Fe content in the SCR catalyst has been measured by atomic absorption spectrometry (Varian Spectra AA 110) after dissolving the sample in an acid solution.

Also, the SCR catalyst has been characterised by EPR recorded at 25 °C and −196 °C on a JEOL JES-FA Series spectrometer at 9.3 GHz (X band) with a 100 kHz field modulation and modulation amplitude of 10 Gauss. Besides, diffuse reflectance UV–Vis (DR UV–Vis) spectra were recorded over the SCR catalyst at ambient atmosphere on a Cary 5E spectrometer equipped with an integrator and a double monochromator.

2.2. Reactivity tests

Catalytic tests have been performed over powder catalysts (sieved at 70–100 μm) loaded in a quartz micro-reactor tube (8 mm I.D.), directly connected to a mass spectrometer (QMS 200, Pfeiffer) for complete analysis of reactants and products including NO, NO_2, N_2O, N_2, H_2 and NH_3 [35–37]. The small delay in the detection of NH_3 was negligible in the results discussed later [38].

The tests have been performed using the single LNT and SCR catalysts, the LNT/SCR physical mixture and the LNT/SCR dual bed (in which the Pt–Ba/Al_2O_3 bed is located upstream the Fe-ZSM-5 SCR bed and is separated by a quartz plug). In the tests with a single catalyst, a sample weight of 60 mg has been used; in the hybrid systems, 60 mg of Pt–Ba/Al_2O_3 plus 60 mg of Fe-ZSM-5 have been loaded into the reactor. A flow of 100 cm^3/min (at 1 atm and 0 °C) has always been used, resulting in a GHSV = 50,000 $cm^3/(g\,h)$ for the single LNT or SCR catalyst and a GHSV = 25,000 $cm^3/(g\,h)$ for both the hybrid systems.

Isothermal Step Concentration (ISC) experiments have been performed, by applying a sequence of lean and rich phases to the reactor and an inert purge in between in order to separate each phase [29,33]. Lean–rich cycles have been carried out at different temperatures (150–350 °C) in the absence and in the presence of CO_2 (0.3% v/v) and H_2O (1% v/v). Briefly, during the lean phase, oxygen (3% v/v) has been admitted at first; then, a pulse of NO (1000 ppm) has been applied to the reactor in flowing He + 3% O_2 until stationary conditions have been reached. Then, after a He purge (that causes desorption of weakly adsorbed NO_x species), catalyst regeneration has been carried out at the same temperature with 2000 ppm H_2 in He (rich phase). Note that NO_x are not present in the rich phase. The catalyst samples have been conditioned by performing few storage/reduction cycles (2–3 cycles); the results reported later refer to conditioned samples. It is noted that, due to the low reactant concentration employed in the experiments, the measured temperature rise upon the lean-fuel rich switch was negligible (<2 °C).

The amounts of NO_x removed and NO_x stored during the lean phase have been calculated as follows:

$$NO_x^{\text{removed,lean phase}} = NO_x^{\text{fed}} - NO_x^{\text{out}} \quad \text{(I)}$$

$$NO_x^{\text{stored,lean phase}} = NO_x^{\text{removed,lean phase}} - N_2^{\text{lean phase}} \quad \text{(II)}$$

In Eq. (I), NO_x^{fed} are the moles of NO_x fed to the reactor, and NO_x^{out} are those exiting the reactor; in Eq. (II) NO_x^{stored} are the moles that remain adsorbed onto the catalyst surface during the lean phase, and $N_2^{leanphase}$ are the moles of N_2 produced from SCR reaction again during the lean phase. The amounts of the N-containing species formed during both the lean and rich phases are expressed in terms of mol/g_{cat} where g_{cat} refer to the weight of Pt–Ba/Al_2O_3 (or Fe-ZSM-5) catalyst (and not to the weight of LNT + SCR catalysts when both components are present).

The N-balance, estimated by comparing the amounts of NO_x removed during the lean phase with those of the N-containing species formed during both the lean and rich phases, typically closed within less than 5–10%.

Finally, the Fe-ZSM-5 catalyst has also been tested in the SCR reaction in the absence and in the presence of CO_2 (0.3% v/v) and H_2O (1% v/v) in the temperature range 150–350 °C. At the investigated temperatures, ammonia has been stored onto the catalyst by admitting 1000 ppm NH_3 in He in a stepwise manner; then, after a He purge, NO (1000 ppm in He + 3% O_2) has been fed to the reactor again in a stepwise manner. This allowed quantifying the NH_3 storage capacity of Fe-ZSM-5 at different temperature and the SCR activity.

2.3. In situ FTIR study

Absorption/transmission IR spectra were run on a Perkin-Elmer FTIR System 2000 spectrophotometer equipped with a Hg–Cd–Te cryo-detector, working in the range of wavenumbers 7200–580 cm^{-1} at a resolution of 2 cm^{-1}. For IR analysis, powder samples were compressed in self-supporting discs (10 mg cm^{-2}) and placed in a commercial heated stainless steel cell (Aabspec) allowing thermal treatments in situ under vacuum or controlled atmosphere and the simultaneous registration of spectra at temperatures up to 600 °C. Experiments were carried out both on the single catalysts (Pt–Ba/Al_2O_3 and Fe-ZSM-5) and on the LNT/SCR physical mixture.

Before the measurements, the samples were treated at 500 °C in vacuum and dry oxygen in order to clean the surface from adsorbed species. For Pt–Ba/Al_2O_3 catalyst and physical mixture of Pt–Ba/Al_2O_3 and Fe-ZSM-5 (1/1 w/w), after this preliminary activation, three storage-reduction cycles at 350 °C in NO_2 and H_2, followed again by outgassing and oxidation at 500 °C, were necessary to convert a large part of the very stable barium carbonate phase [39] into the oxide phase (catalyst conditioning). After these activation/conditioning stages, the samples were cooled down to 250 °C in oxygen and outgassed before the admission of the chosen atmosphere: NO/O_2 mixture (1:4, p_{NO} = 5 mbar), H_2 (5 mbar) or NH_3 (5 mbar). The spectra recorded during the interaction with a gas are reported as difference spectra in the figures: the spectrum subtracted is always that recorded after the activation/conditioning treatment.

3. Results and discussion

3.1. Catalyst characterisation

The specific surface area of the commercial alumina sample after calcination at 700 °C is near 200 m^2/g, while a lower value has been measured for the Pt–Ba/Al_2O_3 sample (160 m^2/g). The surface area contraction was accompanied by small change in the pore volume (0.96 cm^3/g for γ-Al_2O_3 and 0.78 cm^3/g for Pt–Ba/Al_2O_3). The pore radius is in the range 90–110 Å (see Table 1).

In the XRD pattern (not reported) of the calcined Pt–Ba/Al_2O_3 catalyst, characteristic peaks of microcrystalline γ-Al_2O_3 (JCPDS 10-425) have been detected along with those of crystalline phases of Ba-carbonate, both orthorhombic and monoclinic [15,40]. The Pt dispersion measured by H_2 chemisorption was near 15%.

The Fe-ZSM-5 sample shows a specific surface area of 300 m^2/g, and a pore volume of 0.11 cm^3/g. The XRD analysis revealed the characteristic peaks of the ZSM-5 zeolite [41]; no reflections of Fe phases have been found. The iron content is near 1%.

The nature and the environment of iron in Fe-ZSM-5 have been investigated by electron paramagnetic resonance spectroscopy. Fig. 1 shows the EPR spectra of the Fe-ZSM-5 zeolite sample recorded at −196 °C and 25 °C. The two EPR spectra are very similar and show four signals at g = 8.1, 4.3, 2.4 and 2.03. These signals are frequently detected in Fe-containing zeolites but their assignment is not straightforward [42–47]. The number and position of EPR signals for Fe(III) species observable in a powder spectrum mainly depend on the local symmetry of these species and their magnetic

Table 1
Morphological characterisation of the catalytic systems.

Catalyst	Surface area (m^2/g)	Pore volume (cm^3/g)	Pore radius (Å)
γ-Al_2O_3	207	0.96	90–110
Pt–Ba/Al_2O_3	160	0.78	90–110
Fe-ZSM-5	300	0.11	7–10

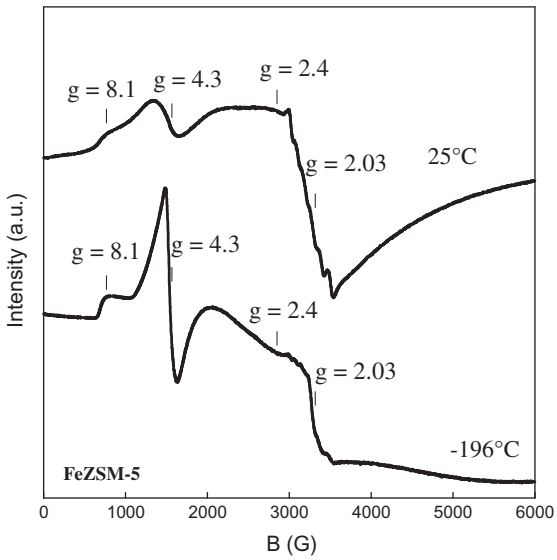

Fig. 1. EPR spectra of Fe-ZSM-5 (X band) recorded at −196 °C and 25 °C and ambient atmosphere.

interactions. As proposed earlier for Fe-containing zeolites [45–50], the signal at $g = 4.3$ may be assigned to tetrahedral Fe(III) ions at lattice sites, that at $g = 8.1$ to isolated Fe(III) ions in penta- and/or octahedral coordination, the broad signal at $g = 2.4$ to iron oxide clusters and the signal at $g = 2.03$ to Fe(III) ions in octahedral environment either isolated or within FeO_x oligomers.

Fig. 2A shows the DR UV–Vis spectrum recorded in ambient atmosphere of the Fe-ZSM-5 sample: a main band at 274 nm is present, assigned to oxygen-to-metal charge transfer (CT) transitions involving isolated Fe(III) ions, in line with literature reports [51–57]; in the inset of Fig. 2A, a very small shoulder near 480 nm is observed in the tail of the band in the visible region, which may suggest the presence of very small amounts of FeO_x oligomers [51–53], in line with EPR results.

To summarise, according to EPR and DR UV–Vis results, Fe(III) ions are present mainly in framework tetrahedral positions and, in appreciable amounts, in octahedral coordination. FeO_x oligomers may also be present in very small amounts.

In Fig. 2B, the FTIR spectrum of Fe-ZSM-5 in the hydroxyl stretching region after outgassing and oxidation at 500 °C is reported. Three main peaks are present at 3740, 3650 and 3600 cm^{-1} assigned to isolated silanol groups, hydroxyls bridged on Si and Fe atoms and hydroxyls bridged on Si and Al atoms, respectively [51,58]. In particular, the absorption at 3650 cm^{-1} confirms the presence of framework Fe(III) ions evidenced by EPR and DR UV–Vis spectroscopy.

3.2. Catalytic activity and complementary in situ FTIR study

3.2.1. NSR cycle over Pt–Ba/Al_2O_3 at 250 °C

The results obtained during ISC experiments in which a storage-reduction cycle was performed over the conditioned Pt–Ba/Al_2O_3 (LNT) sample at 250 °C are shown in Fig. 3. Quantitative data calculated from Fig. 3 are reported in Table 2 and 3.

3.2.1.1. Absence of $CO_2 + H_2O$. Upon NO admission to the reactor ($t = 0$ s, Fig. 3A), the NO outlet concentration presented a dead time (102 s) and then rapidly increased with time, finally reaching a steady state level. The evolution of water, due to the uptake of NO_x at $Ba(OH)_2$, and of NO_2, due to NO oxidation, was also observed, in line with the behaviour of this catalyst previously reported [15,19]. The activity in the oxidation of NO to NO_2 is comparable to that reported in the literature. Indeed, experiments performed at 150 °C show a TOF of 4 s^{-1}, which is in line with the data reported by McCabe et al. [59] for a Pt-catalyst with a comparable Pt dispersion at this temperature.

When the NO feed is switched off, a tail is observed in the NO_x concentration due to the desorption of weakly adsorbed NO_x species [19]. The amounts of stored NO_x (NO_x^{stored}) after NO shutoff are near 4.29×10^{-4} mol/g_{cat} (Table 2), which correspond to 17.6% of the Ba loading assuming the formation of $Ba(NO_3)_2$.

FTIR spectra recorded upon NO/O_2 admission at 250 °C on the Pt–Ba/Al_2O_3 catalyst (Fig. 3C) revealed at first the presence of nitrite species (band at 1220 cm^{-1}), which grow until 2 min of contact and then are progressively oxidised into nitrates (bands at 1545, 1416, 1328 and 1035 cm^{-1}), as already reported [16]. At

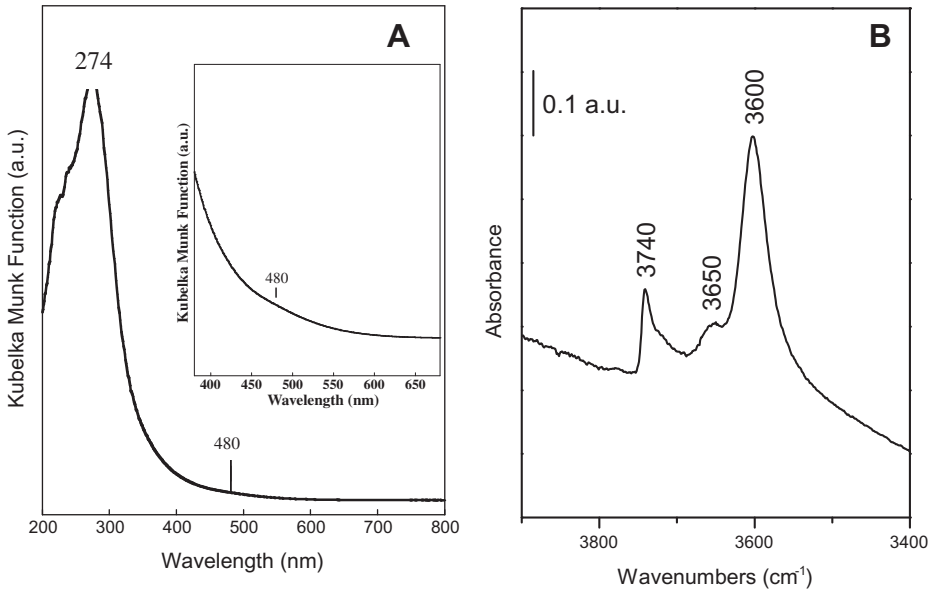

Fig. 2. Spectra of Fe-ZSM-5: (A) DR UV–Vis spectrum recorded at ambient atmosphere and (B) FTIR spectrum in the hydroxyl stretching region after outgassing and oxidation at 500 °C.

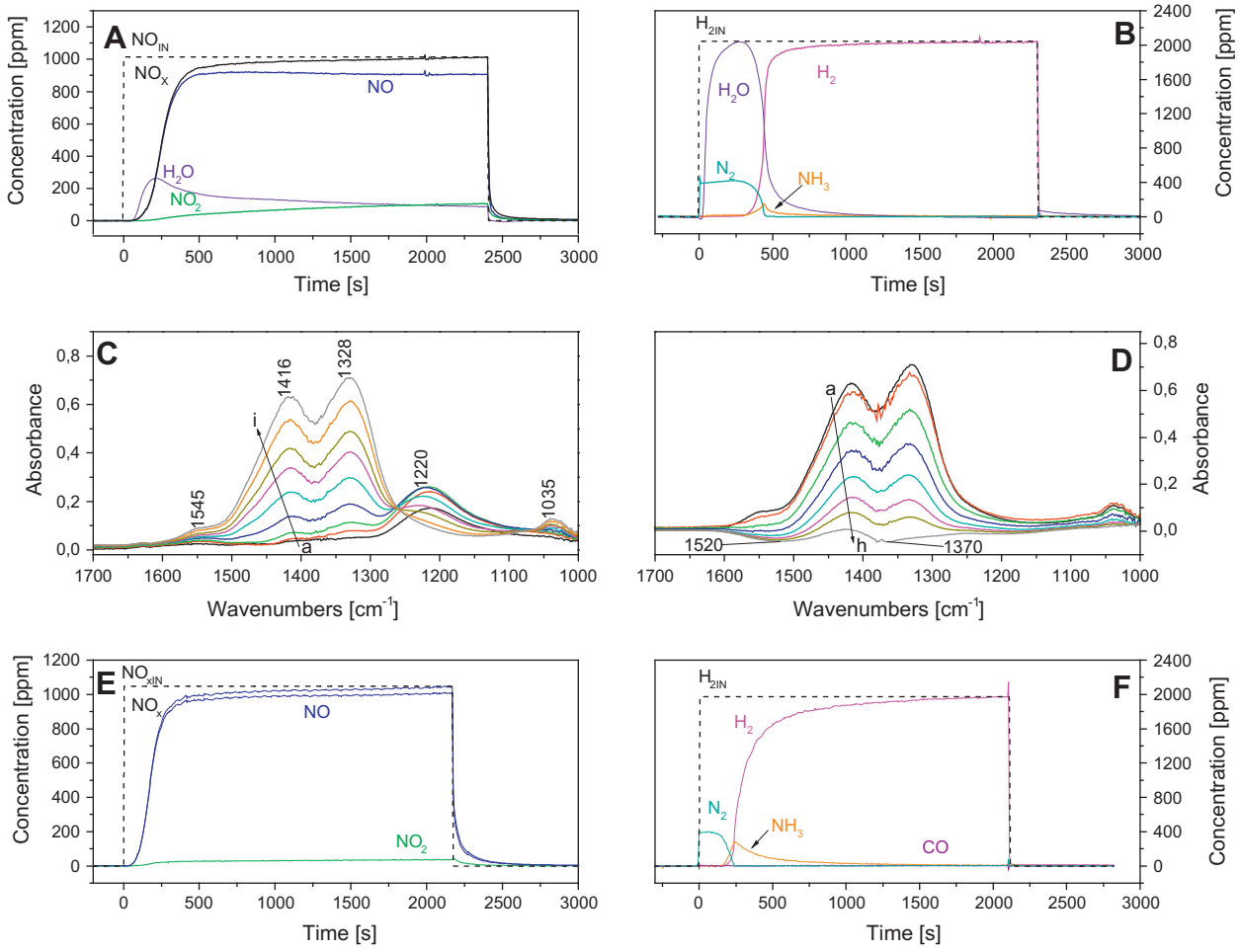

Fig. 3. Lean–rich cycle carried out at 250 °C over LNT Pt–Ba/Al_2O_3 catalyst. (A) ISC experiment, lean phase: 1000 ppm NO in He + O_2 (3%v/v); (B) ISC experiment, rich phase: 2000 ppm H_2 in He; catalyst loading 60 mg, total flow rate 100 cm^3/min (at 1 atm and 0 °C); (C) FTIR spectra recorded upon admission of NO/O_2 (1:4) mixture at 250 °C for 30 s (curve a), 1 min (curve b), 2 min (curve c), 5 min (curve d), 10 min (curve e), 15 min (curve f), 20 min (curve g), 30 min (curve h) and 40 min (curve i); (D) FTIR spectra recorded during the NO_x reduction at 250 °C at increasing contact time: curve a, spectrum of the NO_x stored by NO/O_2 at 250 °C, evacuated at 250 °C; curves b–h, spectra recorded upon H_2 (5 mbar) interaction for 15 s (curve b), 30 s (curve c), 1 min (curve d), 2 min (curve e), 5 min (curve f), 15 min (curve g) and 30 min (curve h); (E) ISC experiment, lean phase: 1000 ppm NO in O_2 (3% v/v) + CO_2 (0.1% v/v) + H_2O (1% v/v) + He; (F) ISC experiment, rich phase: 2000 ppm H_2 in CO_2 (0.1% v/v) + H_2O (1% v/v) + He; catalyst loading 60 mg, total flow rate 100 cm^3/min (at 1 atm and 0 °C).

Table 2
Quantitative analysis of ISC experiments performed over the LNT, LNT + SCR physical mixture and LNT/SCR dual bed configurations in the absence of CO_2 and H_2O. Experimental conditions: T = 250 °C; lean phase NO (1000 ppm) in O_2 (3% v/v) + He; rich phase H_2 (2000 ppm) in He; catalyst weight 60 mg LNT (or 60 mg LNT + 60 mg SCR); total flow rate 100 cm^3/min (at 1 atm and 0 °C). mol/g_{cat} refers to LNT Pt–Ba/Al_2O_3 weight.

Catalyst configuration	LNT	LNT + SCR (physical mixture)	LNT/SCR (dual bed)
NO_x breakthrough time (s)	102	0	212
NO_x removed (mol/g_{cat}) according to Eq. (I)	4.29 × 10–4	5.12×10^{-4}	4.72×10^{-4}
NO_x^{stored} (mol/g_{cat}) according to Eq. (II)	4.29×10^{-4}	4.34×10^{-4}	4.23×10^{-4}
N (N_2 + N_2O + NO + NO_2)* at O_2 admission (mol/g_{cat})	0	1.42×10^{-4}	0
N_2^{lean} (mol/g_{cat})**	0	0.78×10^{-4}	0.49×10^{-4}
N_2^{rich} (mol/g_{cat})***	1.93×10^{-4}	0.509×10^{-4}	2.09×10^{-4}
NH_3 slip (mol/g_{cat})	0.57×10^{-4}	0.70×10^{-4}	0.14×10^{-4}
N-balance	0.97	0.92	0.96

* Moles of N-containing species formed upon O_2 admission.
** N_2 formed during the lean phase.
*** N_2 formed during the rich phase.

the end of the storage, only nitrates are present, mainly of ionic type ($\nu_{NO3,\ asym.}$ mode split at 1416 and 1328 cm^{-1} and $\nu_{NO3,\ sym.}$ mode at 1035 cm^{-1}).

These data parallel our previous studies [15,16] on the pathways for NO_x storage over alumina supported Pt–Ba in the absence of water and CO_2. In the presence of NO/O_2 mixtures, NO is oxidised by O_2 at the Pt–BaO borders to form nitrites ('nitrite route'), according to the following global stoichiometry:

$$2NO + 1/2O_2 + O^{2-} \rightarrow 2NO_2^- \quad (6)$$

Table 3
Quantitative analysis of ISC experiments performed over the LNT, LNT+SCR physical mixture and LNT/SCR dual bed configurations in the presence of CO_2 and H_2O. Experimental conditions: $T = 250$ °C; lean phase NO (1000 ppm) in O_2 (3% v/v) + CO_2 (0.1% v/v) + H_2O (1% v/v) + He; rich phase H_2 (2000 ppm) in CO_2 (0.1% v/v) + H_2O (1% v/v) + He; catalyst weight 60 mg LNT (or 60 mg LNT + 60 mg SCR); total flow rate 100 cm^3/min (at 1 atm and 0 °C). mol/g_{cat} refers to LNT Pt–Ba/Al_2O_3 weight.

Catalyst configuration	LNT	LNT + SCR (physical mixture)	LNT/SCR (dual bed)
NO_x breakthrough time (s)	22	0	62
$NO_x^{removed}$ (mol/g_{cat}) according to Eq. (I)	2.72×10^{-4}	3.23×10^{-4}	3.96×10^{-4}
NO_x^{stored} (mol/g_{cat}) according to Eq. (II)	2.72×10^{-4}	3.07×10^{-4}	2.72×10^{-4}
N (N_2 + N_2O + NO + NO_2)* at O_2 admission (mol/g_{cat})	0	1.77×10^{-4}	0.013×10^{-4}
N_2^{lean} (mol/g_{cat})**	0	0.156×10^{-4}	1.23×10^{-4}
N_2^{rich} (mol/g_{cat})***	0.93×10^{-4}	0.215×10^{-4}	1.35×10^{-4}
NH_3 slip (mol/g_{cat})	1.17×10^{-4}	0.067×10^{-4}	0
N-balance	0.90	0.78	1

* Moles of N-containing species formed upon O_2 admission.
** N_2 formed during the lean phase.
*** N_2 formed during the rich phase.

Nitrite ad-species are then progressively oxidised to nitrates, so that after prolonged exposure only nitrates are present on the catalyst surface.

In parallel with the previously mentioned 'nitrite route', the oxidation of NO to NO_2 on Pt sites by gaseous oxygen can also occur:

$$NO + 1/2O_2 \rightarrow NO_2 \quad (7)$$

The NO_2 is stored on Ba sites in the form of nitrates with no formation of nitrites as stable intermediates detectable by FTIR ('nitrate route'), according to the following global stoichiometry:

$$3NO_2 + O^{2-} \rightarrow 2NO_3^- + NO\uparrow \quad (8)$$

It is worth of note that dedicated experiments performed at different temperatures [16] have shown that 'nitrite route' is predominant at low temperature.

The NO_x stored onto Pt–Ba/Al_2O_3 during the lean phase are readily reduced by hydrogen during the subsequent rich phase (Fig. 3B). H_2 is fully consumed upon admission, and 420 ppm of N_2 is formed together with H_2O (~2000 ppm). In correspondence to the decrease in N_2 concentration, the hydrogen breakthrough is observed and ammonia is also detected while no appreciable amounts of other products (e.g. NO and N_2O) have been measured.

The results in Fig. 3B are in line with the reduction pathway of stored NO_x involving at first the formation of ammonia (reaction (4)) followed by the reaction of ammonia with residual stored nitrates to give N_2 (reaction (5)) [17–19]. Due to the fact that reaction (4) is faster than reaction (5) and to the integral behaviour of the reactor, an H_2 front develops and travels along the reactor. Ammonia is produced at the front, and the regeneration process continues downstream of the hydrogen front due to the reaction of ammonia with stored nitrates (reaction (5)). This fully explains the change of product distribution with time in Fig. 3B.

The reduction of nitrates was also studied by FTIR by admitting hydrogen at 250 °C on the catalyst sample saturated with NO_x at the same temperature (Fig. 3D). The major part of surface nitrates is reduced within 5 min (curve f), and the consumption of nitrates is completed after 20–30 min (curve h). Also, residual carbonates are removed (negative bands at 1520 and 1370 cm^{-1}) at the end of the reduction. It is worth to note that no reduction intermediates are detected by FTIR spectroscopy. In particular: (i) the amount of NH_3 formed remains under the detection limit of the technique in the gas phase (too short optical path of the cell); and (ii) no adsorbed ammonia is detected due to the low NH_3 affinity for the Pt–Ba/Al_2O_3 system, which shows a marked basic character, being the alumina completely covered by the barium phase.

3.2.1.2. Presence of CO_2 + H_2O. Since carbon dioxide and water are present in the exhausts and it is known that they influence the performances of LNT systems [19,60], the effect of the co-presence of CO_2 + H_2O on the NO_x storage-reduction has been investigated.

In Fig. 3E and F, the results of a lean–rich cycle over Pt–Ba/Al_2O_3 at 250 °C in the presence of CO_2 (0.1% v/v) and H_2O (1% v/v) are reported. Data calculated from Fig. 3 are listed in Table 3.

Comparing the storage phase in the presence and in the absence of CO_2 + H_2O (Fig. 3E and A), it appears that the NO_x breakthrough is observed later in a CO_2 + H_2O free environment (102 s vs. 22 s in the presence of CO_2 + H_2O). Consequently, the amounts of stored NO_x are significantly smaller in the presence of CO_2 + H_2O, namely 2.72×10^{-4} vs. 4.29×10^{-4} mol/g_{cat} (compare Tables 2 and 3). As reported by several authors [19,61], the storage of NO_x over barium is more sensitive to CO_2 than to H_2O because $BaCO_3$ is more stable than $Ba(OH)_2$. Therefore, the shorter NO_x breakthrough and the lower amounts of stored NO_x can be ascribed to the formation of Ba carbonates, which inhibit NO_x storage. Besides, Fig. 3E shows that the oxidation of NO to NO_2 is slower in the presence of H_2O and CO_2, since 37 ppm of NO_2 are formed at steady state vs. 56 ppm measured in the absence of H_2O and CO_2 (Fig. 3A). The inhibition has been ascribed in the literature to the presence of water [62,63].

The NO_x stored at 250 °C have been reduced with H_2 in the presence of CO_2 + H_2O at the same temperature (Fig. 3F). H_2 is fully consumed upon admission, and N_2 + H_2O (not shown) are formed due to the reduction of stored NO_x. The hydrogen breakthrough is seen at 151 s, and NH_3 is also detected after 140 s in correspondence to the decrease in N_2 concentration. The amounts of N_2 formed are near 0.93×10^{-4} mol/g_{cat} and are smaller than in the absence of CO_2 and H_2O (1.93×10^{-4} mol/g_{cat}). On the opposite, the amounts of NH_3 produced are higher (1.17×10^{-4} mol/g_{cat} vs. 0.57×10^{-4} mol/g_{cat}). The effect of CO_2 and H_2O on the reduction of stored NO_x has been already investigated in previous papers: it was pointed out that CO_2 reduces the selectivity to N_2 especially at low temperatures [17–19,61]. Indeed, CO_2 inhibits both the reduction of nitrates by hydrogen to give ammonia (reaction (4)) and the subsequent reaction of ammonia with the residual stored nitrates to give nitrogen (reaction (5)) due to the poisoning of Pt by CO as clarified later. The inhibiting effect of CO_2 is stronger over reaction (5), which represents the rate determining step in the overall reduction process.

The reduction does not produce appreciable amounts of other N-containing products (e.g. NO and N_2O) and of CO, which can be formed by the reverse water gas shift (RWGS) reaction:

$$CO_2 + H_2 \Longleftrightarrow CO + H_2O \quad (9)$$

As a matter of fact, the excess of water drives reaction (9) to the left. However, this reaction can occur to a limited extent even at low temperatures, as demonstrated by FTIR experiments, showing that Pt-carbonyls can be formed at temperatures as low as 150 °C

in the presence of a CO_2/H_2 mixture [64]. It is concluded that the inhibiting effect of CO_2 on the reduction at low temperature of the stored NO_x is likely related to the poisoning of the Pt sites by CO formed via the RWGS reaction [19].

3.2.2. NSR cycle over Fe-ZSM-5 at 250 °C

For comparison purposes, NO_x storage-reduction cycles have also been performed over the conditioned Fe-ZSM-5 sample at 250 °C and the results of the storage phase in ISC experiment are shown in Fig. 4A.

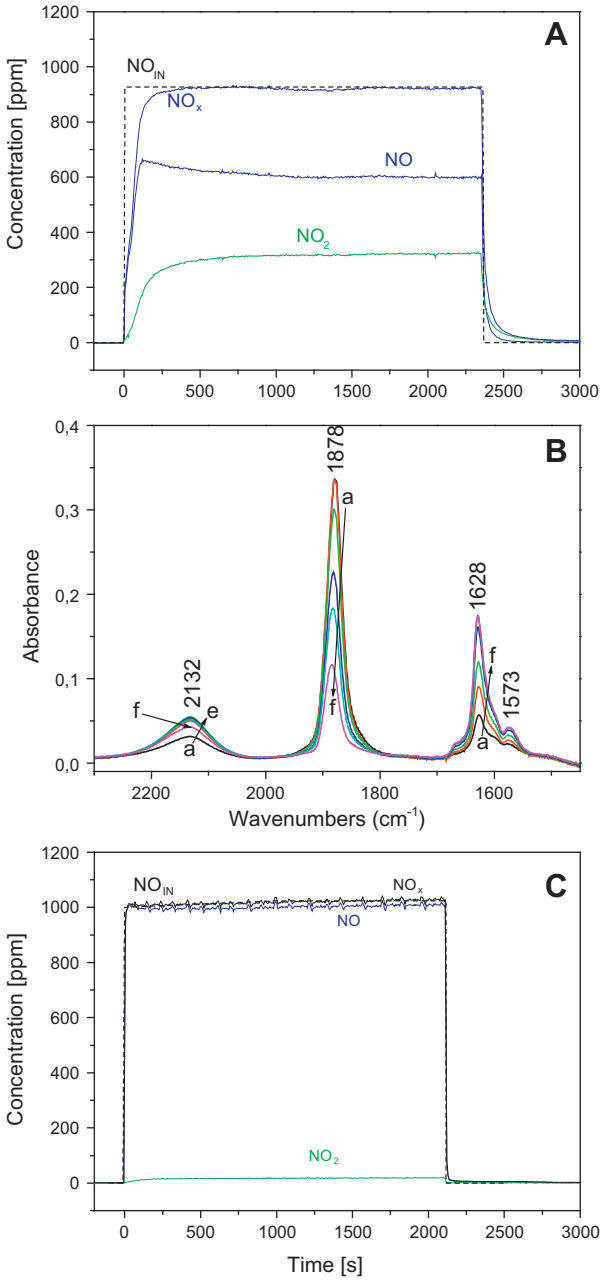

Fig. 4. LNT activity at 250 °C over Fe-ZSM-5 catalyst. (A) ISC experiment, lean phase: 1000 ppm NO in He + O_2 (3%v/v); catalyst loading 60 mg, flow rate 100 cm^3/min (at 1 atm and 0 °C); (B) FTIR spectra recorded upon admission of NO/O_2 (1:4) mixture at 250 °C for 30 s (curve a), 2 min (curve b), 5 min (curve c), 10 min (curve d), 15 min (curve e), 30 min (curve f); (C) ISC experiment in the presence of CO_2 and H_2O: lean phase 1000 ppm NO in O_2 (3% v/v) + CO_2 (0.1% v/v) + H_2O (1% v/v) + He; catalyst loading 60 mg, flow rate 100 cm^3/min (at 1 atm and 0 °C).

Upon admission of NO, the NO_x concentration does not present a dead time and reaches the inlet value quickly after about 200 s, in line with previous observation at 200 °C [33]. The formation of NO_2 up to 324 ppm after near 2300 s is observed, due to the oxidation of NO at Fe sites [65], as evidenced by FTIR measurements reported in the following. The NO trace shows a slight maximum before 200 s, which is likely due to the oxidation of NO to NO_2 (reaction (7)) and the subsequent NO_2 disproportion to give nitrates and gas phase NO (reaction (8)).

The amounts of NO_x that have been stored are low, near 0.42×10^{-4} mol/g_{cat}, in line with previous reports [33,66]. In the subsequent rich phase (not shown), the small amounts of stored NO_x are reduced to N_2, NO and NO_2; very small amounts of NH_3 have also been observed.

These results and the occurrence of reactions (7) and (8) have been confirmed by FTIR spectra recorded at increasing contact time after NO/O_2 admission at 250 °C (Fig. 4B). Immediately after the admission of NO/O_2 (curve a), the presence of a band at 1878 cm^{-1} related to Fe^{3+}(NO) complex is observed along with small amounts of NO^+ (band at 2132 cm^{-1}) and NO_3^- species (main peaks at 1628 cm^{-1} and 1573 cm^{-1} assigned to $\nu_{N=O}$ of bidentate nitrates), in line with literature reports [58,67–70]. By increasing the contact time until 30 min (curves b–f): (i) the Fe^{3+}(NO) band is gradually consumed; (ii) absorptions related to NO_3^- species gradually increase; and (iii) the absorption related to NO^+ increases until 15 min then decreases. The formation of NO^+ and NO_3^- species is ascribed to the occurrence of the NO_2 dismutation reaction:

$$2NO_2 \rightarrow NO_3^- + NO^+ \quad (10)$$

NO_2 is obtained by oxidation of NO activated over Fe sites, as evinced from the erosion of the band at 1878 cm^{-1} related to Fe^{3+}(NO) species. Reaction (10) can be followed by the reaction:

$$NO^+ + NO_2 + O^{2-} \rightarrow NO_3^- + NO\uparrow \quad (11)$$

Reaction (11), once combined with reaction (10), gives the overall stoichiometry of reaction (8). Accordingly, NO^+ represents a reaction intermediate in the formation of surface nitrates, so that the band at 2132 cm^{-1} associated to NO^+ species shows a maximum with time in Fig. 4B, while the bands at 1628 cm^{-1} and 1573 cm^{-1} associated to nitrate ad-species increase continuously with time.

ISC measurements of NO_x storage-reduction cycles have also been performed in the presence of CO_2 + H_2O at the same temperature, and the storage phase is reported in Fig. 4C.

Upon admission, NO is immediately detected at the reactor outlet without breakthrough. NO_2 is not observed, indicating that the co-presence of CO_2 and H_2O strongly inhibits the oxidation of NO over Fe sites, in line with the results reported by Kröcher et al. [71] on the inhibiting effect of water on the NO oxidation capability of Fe-ZSM-5.

3.2.3. SCR cycle over Fe-ZSM-5 at 250 °C

The Fe-ZSM-5 sample has also been tested in the SCR reaction at 250 °C by performing ISC experiments where at first NH_3 and then NO are fed in a stepwise manner to the reactor in the presence of excess O_2 and with an inert purge in between. The results of the ISC experiments are shown in Fig. 5A and B. Upon admission, NH_3 is completely adsorbed onto the zeolite catalyst for 240 s (Fig. 5A); when a steady state NH_3 concentration has been reached, the ammonia feed is closed and a large tail is observed due to the desorption of weakly bound ammonia. Still the amounts of NH_3 that remain adsorbed onto Fe-ZSM-5 before admission of O_2 (t = 4000 s in Fig. 5A or t = −1000 s in Fig. 5B) are large, being near 8.08×10^{-4} mol/g_{cat}. Water is also released from the catalyst surface upon NH_3 adsorption, in line with the tendency of acid catalyst

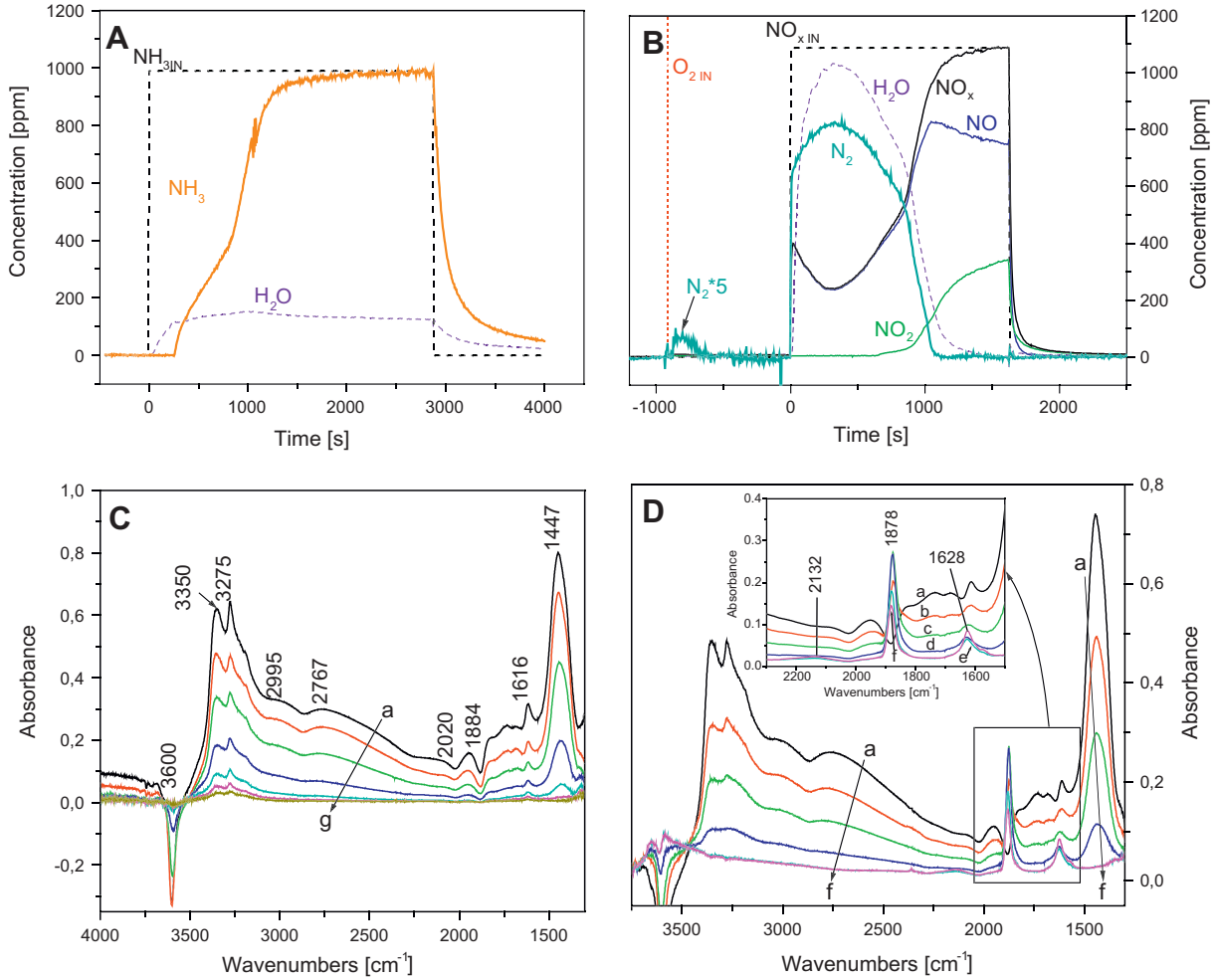

Fig. 5. SCR activity at 250 °C over Fe-ZSM-5 catalyst. (A) ISC experiment, rich phase: 1000 ppm NH_3 in He; (B) ISC experiment, lean phase: 1000 ppm NO in He + O_2 (3% v/v). Catalyst loading 60 mg, flow rate 100 cm^3/min (at 1 atm and 0 °C). (C) FTIR spectra recorded upon admission of NH_3 (5 mbar) at 250 °C (curve a) and subsequent evacuation at 250 °C (curve b), 300 °C (curve c), 350 °C (curve d), 400 °C (curve e), 450 °C (curve f) and 500 °C (curve g). (D) FTIR spectra recorded after NH_3 adsorption and evacuation at 250 °C (curve a) and upon subsequent admission of NO/O_2 mixture (1:4, p_{NO} = 5 mbar) at 250 °C for 30 s (curve b), 1 min (curve c), 2 min (curve d), 5 min (curve e) and 10 min (curve f).

to retain water and with the more basic character of ammonia with respect to water.

After the NH_3 storage, O_2 (3% v/v) at first and then NO (1000 ppm) in the presence of oxygen were admitted to the reactor (Fig. 5B). A small N_2 peak is observed when oxygen was fed (at $t = -1000$ s, dot red[1] line in Fig. 5B) due to ammonia oxidation, which corresponds to 0.2% of the amounts of stored NH_3. Upon admission at $t = 0$ s, NO is immediately consumed to a large extent and N_2 and H_2O are formed due to the occurrence of the standard and fast SCR reactions (1) and (2). The amounts of N_2 produced (8.7×10^{-4} mol/g_{cat}) compare well to the amounts of stored NH_3 (8.08×10^{-4} mol/g_{cat}).

It is worth noting that the concentration of NO in Fig. 5B shows a minimum, corresponding to a maximum in the N_2 production. This is likely due to the inhibition of ammonia at high coverage on the SCR reactions. The inhibition of ammonia at high coverage and low temperatures has been documented for traditional vanadia-tungsta-titania by Tronconi and co-workers [72] and was ascribed to competition between NO and ammonia for adsorption onto the active sites. The inhibition of the SCR reaction by excess ammonia at low and intermediate temperatures was also observed over Fe-ZSM-5 and was explained by the reducing properties of ammonia converting Fe^{3+} to Fe^{2+} or by preventing the re-oxidation of Fe^{2+} [73].

NO_2 is detected in correspondence with the decrease in the concentration of nitrogen and water and with the increase in NO concentration, due to oxidation of NO. The appearance of NO_2 at the reactor exit several minutes after detection of NO (compare Fig. 5B with Fig. 4A) suggests that during the early minutes NO_2 could be involved in the fast SCR reaction (2), which is known to be faster than the standard SCR reaction (1) [10,74]. Alternatively, since NO_2 is observed at the reactor exit only when adsorbed ammonia has been fully depleted, this could be due to the inhibition of ammonia stored over Fe sites on the oxidation of NO to NO_2 [75], in line with the inhibiting effect of water on NO oxidation already mentioned (see Fig. 4C) [71], or to the fact that ammonia intercepts and reduces intermediate species in NO oxidation.

The occurrence of both the standard and the fast SCR reactions on Fe-ZSM-5 is well documented in the literature. Schwidder et al. [55] have provided clear evidence for the participation of Fe sites in the SCR reactions. The authors showed that the SCR reactions of NO (standard SCR) and of NO/NO_2 mixtures (fast SCR) over Fe-ZSM-5 proceed at different Fe sites. Whereas standard SCR occurs at both isolated and oligomeric Fe oxo-sites, fast SCR requires only a small

[1] For interpretation of colour in Figs. 3–10, the reader is referred to the web version of this article.

concentration of isolated Fe sites. Notably, EPR and UV–Vis results of catalyst characterisation discussed previously show the presence of different Fe sites in the investigated Fe-ZSM-5 catalyst, so that it can be argued that different iron sites could participate differently to the SCR reactions in Fig. 5B.

Together with the appearance of NO_2 at the reactor exit, a maximum in the concentration of NO is apparent in Fig. 5B, which, as already discussed, is likely due to the oxidation of NO to NO_2 followed by NO_2 disproportion to give nitrates, NO^+ ad-species and gas phase NO (reaction 7, 8, and 11). The adsorption of NH_3 on Fe-ZSM-5 and its subsequent interaction with NO/O_2 mixture at 250 °C has also been studied by FTIR spectroscopy, and the results are reported in Fig. 5C and D, respectively. In Fig. 5C, the FTIR spectra recorded upon NH_3 admission at 250 °C and subsequent evacuation at increasing temperature are reported. Immediately after NH_3 admission (curve a), intense bands related to coordinatively bonded and protonated NH_3 (ammonium ion, NH_4^+) appear. In particular, ammonia coordinated at Lewis acid sites (Al^{3+} and Fe^{3+}) shows absorptions in the region 3500–3100 cm^{-1} assigned to ν_{N-H} modes and at 1616 cm^{-1} assigned to $\delta_{N-H,asym.}$ mode; ammonium ion (NH_4^+) shows absorptions in the region 3000–2250 cm^{-1} assigned to ν_{N-H} modes and at 1447 cm^{-1} assigned to $\delta_{N-H,asym}$ mode [76,77]. The spectral region of N—H stretching vibrations is relatively complex, because the distortion of the NH_3 molecule upon coordination leads to a splitting of the $\nu_{N-H,asym}$ mode and to the activation of the $\nu_{N-H,sym}$ mode; furthermore, a Fermi resonance is present between the first overtone of $\delta_{N-H,asym.}$ and $\nu_{N-H,sym.}$ modes.

The NH_4^+ species are formed by subtracting protons from the Brønsted acid sites with the highest acid strength. These sites show the stretching vibrational mode at 3600 cm^{-1} (Fig. 2B). As a consequence, in the difference spectra of Fig. 5C, a negative peak appears at 3600 cm^{-1}. Besides, other negative peaks are present at 2020 and 1884 cm^{-1} related to overtones and combination vibrations of the zeolite bulk modes, which are perturbed by the ammonia adsorption.

The subsequent outgassing at increasing temperature up to 500 °C evidence high thermal stability of both coordinatively bonded and protonated ammonia. Even if considerable amounts of both ammonia adsorbed species are desorbed already at 250 °C (Fig. 5C, curve b), in agreement with the ISC experiment in Fig. 5A, both species are still present after evacuation at 450 °C (curve f). At 500 °C (curve g), only ammonia coordinated on Lewis acid sites is still present in very low amount.

Then, NH_3 was adsorbed again and outgassed at 250 °C (Fig. 5D, curve a), before interaction at the same temperature with NO/O_2 mixture (Fig. 5D, curves b–f for increasing contact times). Immediately after the NO/O_2 admission, both ammonia coordinated on Lewis acid sites and NH_4^+ species are consumed by the SCR reactions. Until the ammonia is present on the surface, the only observable NO_x surface species is $Fe^{3+}(NO)$, whose band at 1878 cm^{-1} continues to increase in intensity until 2 min (inset of Fig. 5D, curve d).

Note that in the absence of pre-adsorbed ammonia, this band immediately reaches the highest intensity; conversely, in the presence of pre-adsorbed ammonia, the intensity increase in this band at low contact times is low and reveals the presence of ammonia directly bonded onto Fe^{3+} ions.

After 5 min of contact, when adsorbed ammonia is completely consumed, the increase in NO^+ and nitrate bands at 2132 and 1628 cm^{-1}, respectively, is observed contemporary to the erosion of the peak related to $Fe^{3+}(NO)$ species, in line with the results obtained with NO/O_2 and without pre-adsorbed ammonia.

3.2.4. NSR cycle over LNT+SCR physical mixture at 250 °C

The physical mixture of $Pt–Ba/Al_2O_3$ and Fe-ZSM-5 has been tested under the same ISC conditions employed in the study of the single LNT and SCR catalysts, and the results of a lean–rich sequence at steady cyclic conditions are shown in Fig. 6. Data calculated from Fig. 6 are reported in Tables 2 and 3.

3.2.4.1. Absence of $CO_2 + H_2O$. Upon O_2 admission ($t = -1000$ s in the Fig. 6A), a remarkable spike in the production of N_2, N_2O and NO (1.42×10^{-4} mol/$g_{cat.}$ of N-species, see Table 2 and Fig. 7A) is observed due to the oxidation of ammonia stored onto the Fe-ZSM-5 catalyst during the previous rich phase. This feature will be discussed more in detail later, when the effect of $CO_2 + H_2O$ will be addressed.

At $t = 0$, NO is added to the flow and its concentration slowly increases with time without any time delay and shows a maximum at 590 s and then decreases. The production of N_2 (near 0.78×10^{-4} mol/g_{cat}) is also apparent immediately upon admission of NO, due to the SCR reactions of NO_x with ammonia, which has been stored on the Fe-ZSM-5 catalyst during the previous rich phase, as it is confirmed by the FTIR study presented later.

Notably, the absence of a time delay in nitrogen production is related to the arrangement of the hybrid system. Indeed, in the physical mixture, the Fe-ZSM-5 particles are well mixed with the $Pt–Ba/Al_2O_3$ particles, so that the NO_x storage on the $Pt–Ba/Al_2O_3$ particles and the reactions of NO_x with NH_3 on the Fe-ZSM-5 particles to form N_2 occur simultaneously. In view of this, no time delay in nitrogen production is observed over this hybrid system.

NO_2 is also observed after the nitrogen peak: its concentration increases with time to the level of 462 ppm after 2450 s. The delay in the NO_2 detection has been already discussed in the case of SCR cycle over Fe-ZSM-5. The absence of a significant delay in NO concentration and the maximum observed in Fig. 6A might be due to the formation of NO_2 in large amounts over the Fe-ZSM-5 particles followed by NO_2 disproportion to give nitrates and gas phase NO. The features observed in Fig. 6A are in line with the results reported in Ref. [33] at a slightly different temperature.

The amounts of NO_x removed over this hybrid system, which in total are near 5.12×10^{-4} mol/g_{cat}, are due to SCR reactions over Fe-ZSM-5 (0.78×10^{-4} mol/g_{cat}) and to NO_x storage onto $Pt–Ba/Al_2O_3$ (4.34×10^{-4} mol/g_{cat}). Indeed, the amounts of NO_x stored on the $Pt–Ba/Al_2O_3$ particles in the physical mixture compare well with those measured over the single LNT catalyst (4.34×10^{-4} vs. 4.29×10^{-4} mol/g_{cat}), which eventually confirms that the storage of NO_x occurs primarily onto $Pt–Ba/Al_2O_3$ and that the presence of Fe-ZSM-5 and its extensive contact with the LNT catalyst do not influence significantly the amounts of stored NO_x. However, a minor contribution due to NO_x storage onto the SCR catalyst is possible.

We conclude that the LNT+SCR physical mixture show a higher NO_x removal thanks to two contributions, i.e., the storage of NO_x over LNT catalyst and the occurrence of the SCR reactions over SCR catalyst. However, we note that significant amounts of ammonia stored onto Fe-ZSM-5 catalyst particles during the previous rich cycle are oxidised upon oxygen admission and, because of this, they cannot take part in the SCR reactions during the lean phase.

The NO_x stored at 250 °C have been reduced with H_2 at the same temperature (Fig. 6B). The H_2 concentration trace shows a complex shape and increases slowly with time, reaching the inlet value after 2000–2500 s. Water is observed in large amounts as a product of reduction, while only small amounts of N_2 and NH_3 are detected (0.51×10^{-4} and 0.70×10^{-4} mol/g_{cat}, respectively). Besides, the ammonia slip over the LNT+SCR physical mixture is higher than that observed over the single LNT catalyst, in spite of the presence of the Fe-ZSM-5 system component with a strong acidic character. This point will be discussed later, when the effect of temperature will be addressed.

The overall H_2 consumption (30.3×10^{-4} mol/g_{cat}) is much higher than expected from the net production of N_2 and of NH_3

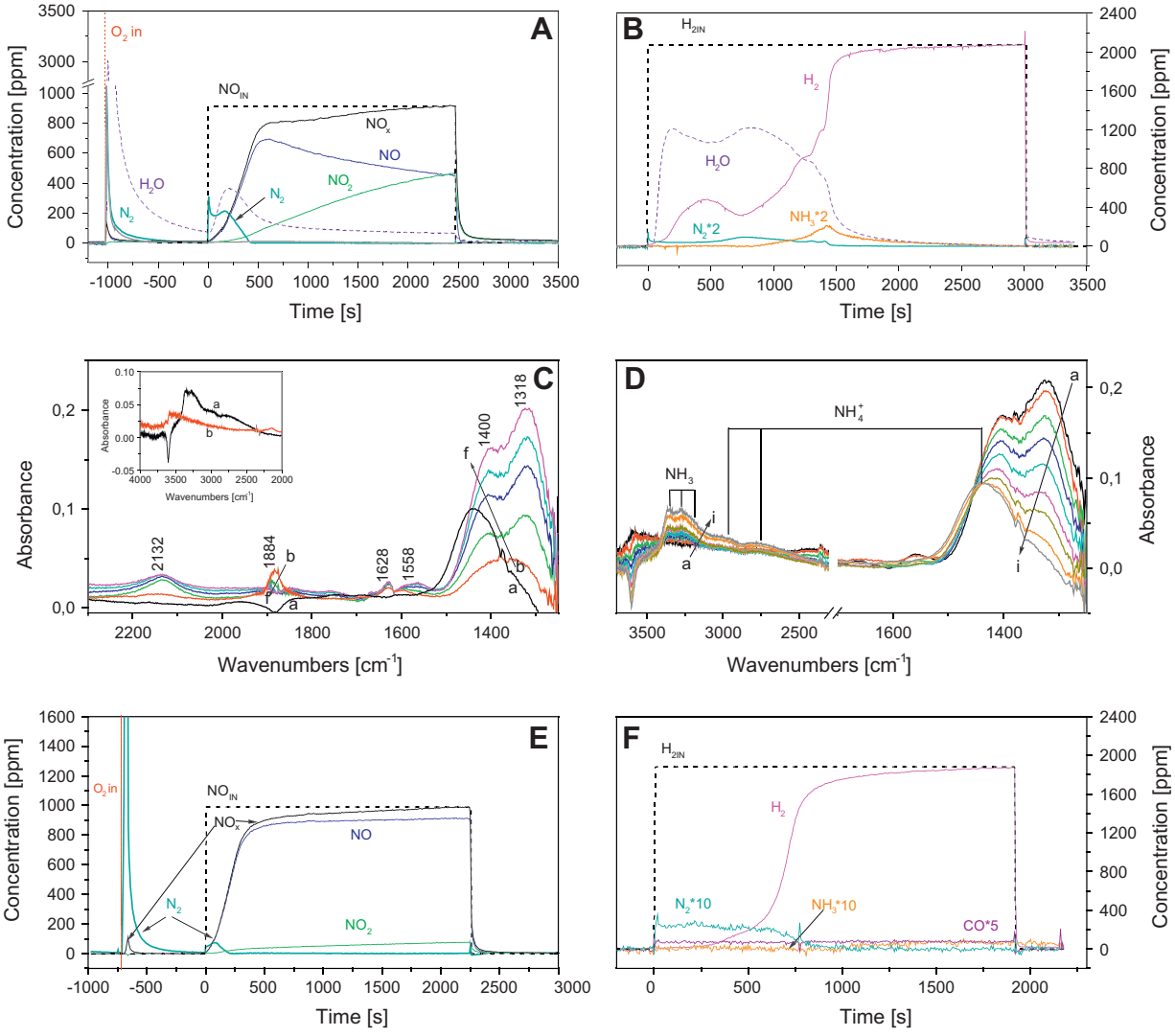

Fig. 6. Lean–rich cycles carried out at 250 °C over LNT + SCR physical mixture. (A) ISC experiment, lean phase: 1000 ppm NO in He + O_2 (3%v/v); (B) rich phase 2000 ppm H_2 in He. Catalyst loading 60 mg LNT + 60 mg SCR, flow rate 100 cm^3/min (at 1 atm and 0 °C). (C) FTIR spectra recorded after a storage-reduction cycle (curves a) and subsequent admission of NO/O_2 mixture (1:4, p_{NO} = 5 mbar) at 250 °C for 30 s (curves b), 5 min (curve c), 10 min (curve d), 15 min (curve e) and 30 min (curve f) (catalyst loading 1/1 LNT/SCR w/w). (D) FTIR spectra recorded during the NO_x reduction at 250 °C at increasing contact time: curve a, spectrum of the NO_x stored by NO/O_2 at 250 °C, evacuated at 250 °C; curves b–i, spectra recorded upon H_2 (5 mbar) interaction for 30 s (curve b), 1 min (curve c), 2 min (curve d), 5 min (curve e), 10 min (curve f), 15 min (curve g), 30 min (curve h) and 50 min (curve i) (catalyst loading 1/1 LNT/SCR w/w); (E) ISC experiment, lean phase: 1000 ppm NO in O_2 (3% v/v) + CO_2 (0.1% v/v) + H_2O (1% v/v) + He. (F) ISC experiment, rich phase: 2000 ppm H_2 in CO_2 (0.1% v/v) + H_2O (1% v/v) + He. catalyst loading 60 mg LNT + 60 mg SCR, total flow rate 100 cm^3/min (at 1 atm and 0 °C).

according to the stoichiometry of the reduction of stored nitrates to give ammonia and nitrogen (reactions (4) and (12)):

$$Ba(NO_3)_2 + 8H_2 \rightarrow 2NH_3 + BaO + 5H_2O \quad (4)$$

$$Ba(NO_3)_2 + 5H_2 \rightarrow N_2 + BaO + 5H_2O \quad (12)$$

This is due to the fact that the LNT + SCR physical mixture favours the trapping of ammonia formed by reaction (4) onto Fe-ZSM-5 particles during the rich phase and prevents further reaction of NH_3 with NO_x stored downstream onto the Pt–Ba/Al_2O_3 particles to give N_2 (reaction (5)), in view of effective contact between the particles of the two system components.

The lean–rich cycle over the LNT + SCR physical mixture, with admission of NO/O_2 and then of H_2 at 250 °C, has also been studied by FTIR. Firstly, the NO/O_2 admission has been performed on a system activated at 500 °C and, so, completely free from ammonia adsorbed in the previous rich phase (not reported for sake of brevity). The results obtained upon NO/O_2 admission are exactly the combination of the results obtained over the two single LNT and SCR systems (see Fig. 3C and Fig. 4B): (i) the bands of ionic nitrates ($\nu_{NO3,asym}$ mode split at 1400 and 1318 cm^{-1}) and of bidentate nitrates ($\nu_{N=O}$ mode at 1558 cm^{-1}, the only one visible) increase until saturation onto the Pt–Ba/Al_2O_3 particles; and (ii) the bands of Fe^{3+}(NO) species (ν_{NO} mode at 1884 cm^{-1}) are immediately formed onto the Fe-ZSM-5 particles and are then consumed to give NO_2, whose dismutation causes the increase in the bands of NO^+ species (band at 2132 cm^{-1}, with a maximum) and of nitrate species (main band at 1628 cm^{-1}). It is important to remind that the nitrite species formed at low contact time on the Pt–Ba/Al_2O_3 surface cannot be detected in this case because of the complete absorption of the radiation by the bulk vibrational modes of the zeolite system component.

After reduction, a new lean cycle has been performed and the results are reported in Fig. 6C. Ammonia formed on the LNT particles and adsorbed on Fe-ZSM-5 particles in the previous rich phase is almost completely consumed immediately after NO/O_2 admission. This is evident from the comparison between curve a (spectrum recorded at the end of the previous rich phase) and curve b

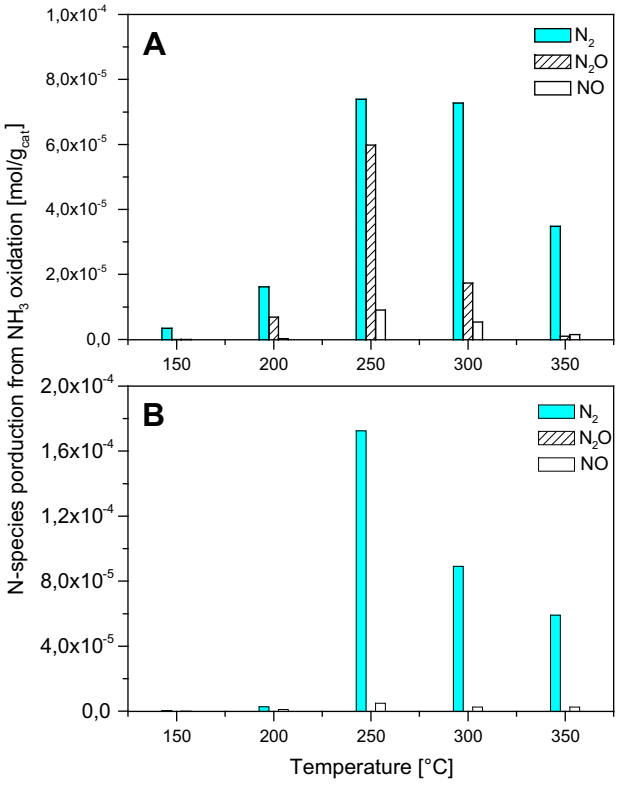

Fig. 7. Oxidation of ammonia upon O_2 admission over LNT/SCR physical mixture configuration (A) in the absence of CO_2 + H_2O and (B) in the presence of CO_2 (0.3% v/v) + H_2O (1% v/v). Other experimental conditions as in Figs. 3, 6 and 8.

(spectrum after 30 s of contact with NO/O_2) both in the region of δ_{N-H} modes (1600–1400 cm^{-1}) and ν_{N-H} modes (3500–2250 cm^{-1}, in the insert of Fig. 6C). Residual NH_4^+ can be revealed after 30 s of contact by the broad band in the region 1500–1250 cm^{-1} (curve b), which is the result of the superimposition of the absorptions related to $\delta_{N-H,asym}$ mode of residual ammonium ion and the split $\nu_{NO3,\ asym.}$ mode of nitrates. At longer contact time, the evolution of surface species is the same observed in the case of the system free from ammonia and already described.

After the interaction with NO/O_2 mixture, H_2 admission (Fig. 6D) at 250 °C causes the gradual reduction of stored NO_x that produced NH_4^+ and adsorbed ammonia, as clearly evidenced by the temporal evolution of bands in the region 1600–1400 cm^{-1} and 3500–2250 cm^{-1}, respectively, and accounts for the consumption of nitrate bands (region 1500–1250 cm^{-1}). This eventually accounts also for the detection of small amounts for N_2 and NH_3 in Fig. 6B.

3.2.4.2. Presence of CO_2 + H_2O. Fig. 6E and F show the ISC results obtained during a lean–rich cycle over the LNT + SCR physical mixture at 250 °C in the co-presence of CO_2 and H_2O. Data calculated from Fig. 6E and F are reported in Table 3.

During the lean phase (Fig. 6E), immediately upon admission of oxygen at $t = -750$ s, a remarkable spike in the production of N_2 (1.72×10^{-4} mol/g_{cat}) and small amount of NO (0.05×10^{-4} mol/g_{cat}) are observed due to oxidation of NH_3. This amount in total and the selectivity to nitrogen are higher than in the absence of CO_2 and H_2O (compare Fig. 7B and A, Tables 3 and 2). The oxidation of ammonia upon admission of oxygen over the LNT + SCR physical mixture can be explained by desorption of ammonia stored during the previous rich phase from the surface of Fe-ZSM-5 particles followed by reaction of ammonia on the surface of Pt–Ba/Al_2O_3 particles, which are in close contact with the Fe-ZSM-5 particles. Indeed, the desorption of ammonia is rate controlling in the ammonia adsorption–desorption process over an acid catalyst surface [78,79] like that of Fe-ZSM-5 while, at the experimental conditions of the present study, the oxidation of ammonia over Fe-ZSM-5 is negligible (see Fig. 5B) but is very effective over Pt–Ba/Al_2O_3 already at 100 °C, as confirmed by dedicated experiments. Accordingly, the oxidation of ammonia over Pt–Ba/Al_2O_3 leads to the consumption of ammonia present in the gas phase and drives the ammonia adsorption–desorption equilibrium towards ammonia desorption. The higher level of ammonia oxidation measured (upon oxygen admission) over the LNT + SCR physical mixture in the presence of H_2O + CO_2 (1.77×10^{-4} mol/g_{cat} in Fig. 6E vs. 1.42×10^{-4} mol/g_{cat} in Fig. 6A) could be explained with the fact that water favours ammonia desorption although to a very small extent, but the effect is amplified by the consecutive oxidation of ammonia.

Note that the extent of ammonia oxidation measured upon oxygen admission is likely related to the modus operandi adopted for the lean–rich cycles (i.e. first admission of O_2 and then of NO) and that other features might be observed using different operating procedures (i.e. co-admission of NO + O_2).

Upon admission at $t = 0$ s, NO is seen at the reactor exit without any time delay (Fig. 6E) together with N_2, that is formed due to the SCR reactions between NO and ammonia, which has been trapped onto the Fe-ZSM-5 catalyst particles during the previous rich phase and has not been oxidised upon oxygen admission. The amounts of nitrogen produced during the lean phase are lower in the presence than in the absence of CO_2 + H_2O (near 0.156×10^{-4} mol/g_{cat} and 0.78×10^{-4} mol/g_{cat}). However, it is worth to note that most of the ammonia that has been trapped during the previous rich phase is oxidised upon oxygen admission, namely 1.77×10^{-4} mol/g_{cat} and 1.42×10^{-4} mol/g_{cat} in the presence and absence of CO_2 + H_2O, respectively.

The amounts of NO_x removed during the lean phase and after the He purge and the oxygen admission are lower due to the inhibiting effect of CO_2 on the NO_x storage (3.23×10^{-4} mol/g_{cat} in Table 3. and 5.12×10^{-4} mol/g_{cat} in Table 2) and to the lower amounts of nitrogen formed in the lean phase (0.156×10^{-4} mol/g_{cat} in Table 3 and 0.78×10^{-4} mol/g_{cat} in Table 2). The lower amounts of N_2 formed during the lean phase in turn are due to the effect of water on ammonia adsorption–desorption, which accounts for the lower amounts of ammonia adsorbed during the rich phase ($(1.77 + 0.156) \times 10^{-4}$ mol/g_{cat} in Table 3 and $(1.42 + 0.78) \times 10^{-4}$ mol/g_{cat} in Table 2) and for the higher amounts of ammonia oxidised upon oxygen admission (1.77×10^{-4} mol/g_{cat} in Table 3 and 1.42×10^{-4} mol/g_{cat} in Table 2).

Finally, Fig. 6E confirms that the oxidation of NO to NO_2 is strongly inhibited in the presence of H_2O and CO_2, since at steady state 77 ppm of NO_2 are formed vs. 462 ppm in the absence of H_2O and CO_2. The evolution of NO_2 is seen after the N_2 peak, due to the participation of NO_2 in the fast SCR reaction or to the inhibition of ammonia on the oxidation of NO to NO_2.

The NO_x stored at 250 °C have been reduced in the presence of CO_2 and H_2O at the same temperature (Fig. 6F). H_2 is fully consumed after its admission until breakthrough that is observed at 232 s. After H_2 admission, very small N_2 and NH_3 peaks are seen. Like in the absence of CO_2 and H_2O, the amounts of N_2 formed and of NH_3 slipped (0.215×10^{-4} mol/g_{cat} and 0.067×10^{-4} mol/g_{cat}, respectively) do not account for H_2 consumption. In fact, large amounts of NH_3 are formed according to reaction (4) and are trapped onto the Fe-ZSM-5 particles; eventually, during the subsequent lean cycle, either they are oxidised upon oxygen admission or react with NO_x according to SCR reactions, as already discussed. No other N-containing products are seen at the reactor exit during the rich phase, and similarly, negligible amount of CO due to the RWGS reaction is detected.

Comparing Fig. 6F with 6B, it clearly appears that lower amounts of N_2 and NH_3 are produced in the presence of $CO_2 + H_2O$ possibly due to the lower amounts of stored NO_x (compare also Tables 3 and 2). The large amounts of NH_3 formed are completely blocked onto the Fe-ZSM-5 particles and do not take part in the subsequent step of the reduction; accordingly, a lower ammonia slip is observed.

3.2.5. NSR cycle over LNT/SCR dual bed at 250 °C

The results obtained in a lean–rich cycle over the LNT/SCR dual bed with the Pt–Ba/Al_2O_3 catalyst located upstream of the Fe-ZSM-5 catalyst are displayed in Fig. 8. Data calculated from Fig. 8 are reported in Tables 2 and 3.

3.2.5.1. Absence of $CO_2 + H_2O$. During the lean period (Fig. 8A), upon admission of NO to the reactor, complete NO uptake is observed until breakthrough, which occurs at 212 s, later than over the single Pt–Ba/Al_2O_3 system (102 s, Fig. 3A); then, the NO_x concentration increases with time. At the end of the lean phase and after the purge in He, higher amounts of NO_x have been removed (4.72×10^{-4} mol/g_{cat}) as compared to the single LNT catalyst (4.29×10^{-4} mol/g_{cat}, Fig. 3A).

The production of N_2 is also apparent in Fig. 8A; the amounts of N_2 produced in the lean phase are estimated near 0.49×10^{-4} mol/g_{cat}. As expected, the amounts of NO_x removed from the gas phase over the LNT/SCR dual bed (4.72×10^{-4} mol/g_{cat}) are similar to those stored onto the single LNT catalyst (4.29×10^{-4} mol/g_{cat}) plus those consumed by the SCR reactions (0.49×10^{-4} mol/g_{cat}), namely 4.78×10^{-4} mol/g_{cat}. On the other hand, the amounts of NO_x stored onto the LNT/SCR dual bed compare well with those stored onto the single LNT (4.23×10^{-4} vs. 4.29×10^{-4} mol/g_{cat}). This confirms that the storage of NO_x occurs primarily on the LNT catalyst, although a minor contribution from the SCR catalyst is possible, in line with the limited storage of NO_x observed over Fe-ZSM-5.

Finally, the amounts of N_2 produced in the lean phase (0.49×10^{-4} mol/g_{cat}) plus the ammonia slip observed during the rich phase (0.14×10^{-4} mol/g_{cat}, as detailed later) compare well with the amounts of NH_3 released from the single Pt–Ba LNT catalyst during the rich phase (Fig. 3B, 0.63×10^{-4} mol/g_{cat} vs. 0.57×10^{-4} mol/g_{cat}). This confirms that N_2 is formed during the lean phase by the SCR reactions between NH_3 stored on the Fe-ZSM-5 catalyst, placed downstream of the LNT bed, during the previous rich phase, and NO_x slipped from the Pt–Ba/Al_2O_3 catalyst bed. It is worth noting that the amounts of NH_3 stored onto the Fe-ZSM-5 are much lower than its storage capacity at the same temperature (0.49×10^{-4} vs. $8.08–8.7 \times 10^{-4}$ mol/g_{cat}).

Fig. 8A also shows that NO_2 is detected after the nitrogen peak, in line with the occurrence of the fast SCR reaction (2) or the ammonia inhibition on the NO–NO_2 oxidation, as already discussed. Accordingly NO_2 is observed at the reactor exit only when adsorbed ammonia has been fully depleted. The production of NO_2 increases with time and after 2000 s is high (344 ppm) but apparently has not reached yet a steady state level. Together with the appearance of NO_2, a maximum in the concentration of NO is observed in Fig. 8A, due to the oxidation of NO to NO_2 followed by NO_2 disproportion to give nitrates and gas phase NO.

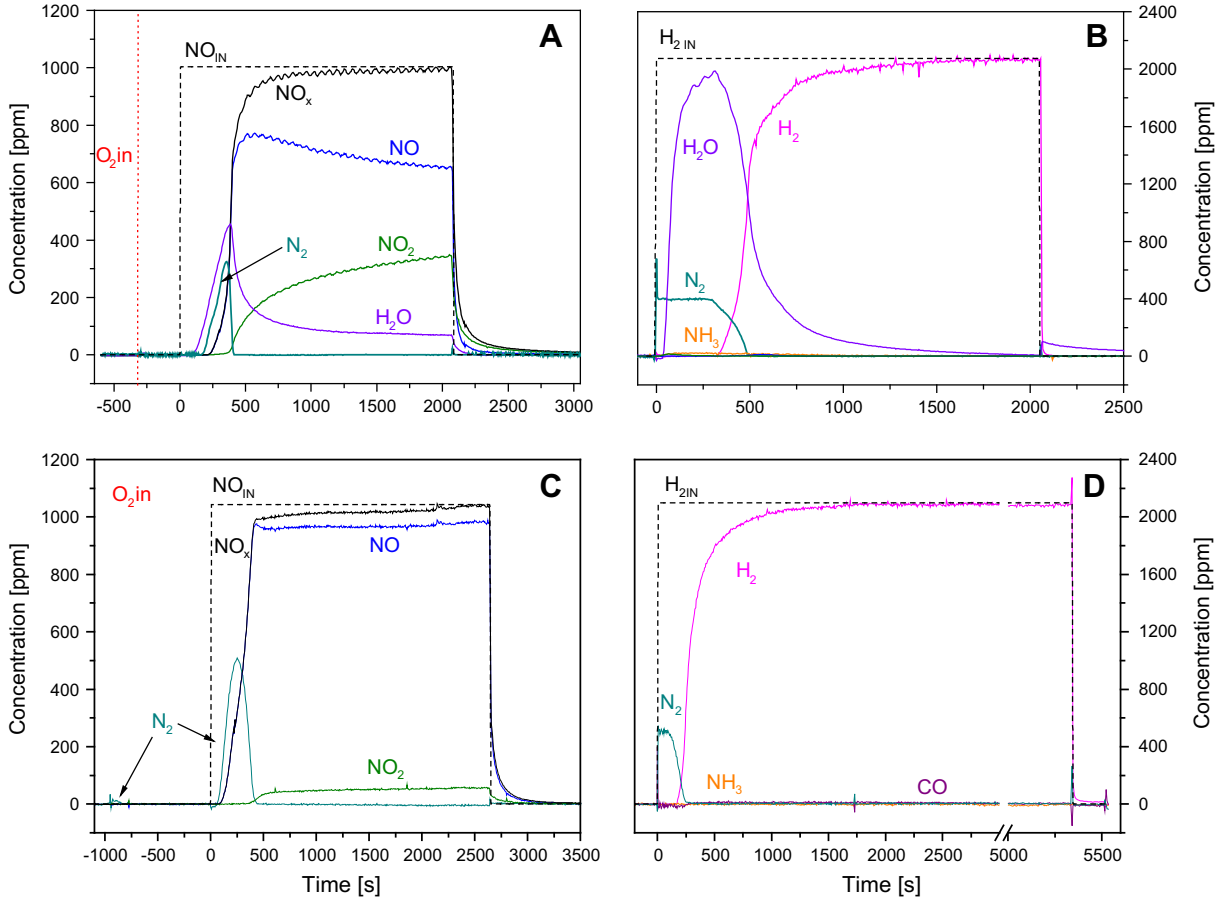

Fig. 8. ISC experiments with lean–rich cycles carried out at 250 °C over LNT/SCR dual bed. (A) Lean phase: 1000 ppm NO in He + O_2 (3%v/v); (B) rich phase: 2000 ppm H_2 in He; (C) lean phase 1000 ppm NO in O_2 (3% v/v) + CO_2 (0.1% v/v) + H_2O (1% v/v) + He; D) rich phase: 2000 ppm H_2 in CO_2 (0.1% v/v) + H_2O (1% v/v) + He; catalyst loading 60 mg LNT + 60 mg SCR, total flow rate 100 cm^3/min (at 1 atm and 0 °C).

It is worth to note that the delay in N_2 production is related to the arrangement of the hybrid system with the Pt–Ba/Al_2O_3 catalyst bed placed upstream of the Fe-ZSM-5 catalyst bed. In fact, NO_x reach the Fe-ZSM-5 catalyst bed only after the NO_x breakthrough over the LNT bed, giving N_2 by reaction with stored ammonia. However, the NO_x breakthrough has been observed at 102 s over Pt–Ba/Al_2O_3, while N_2 has been observed from 150 s over the hybrid system in Fig. 8A. The disagreement between the two time delays is due to the variance of the NO_x breakthrough over Pt–Ba/Al_2O_3 observed in our lab during replicated experiments [29,33].

Finally, negligible amounts of adsorbed NH_3 are oxidised to N_2 upon oxygen admission to the reactor (at $t = -250$ s, Fig. 8A). This is due to the fact that desorbed NH_3 cannot be oxidised over the LNT catalyst, which is placed upstream; accordingly, the oxidation of ammonia occurs to a negligible extent with respect to the LNT/SCR physical mixture where Pt and Fe particles are well mixed. It is also noted that lower amounts of ammonia are stored onto the Fe-ZSM5 catalyst bed in this case.

The NO_x stored at 250 °C have been reduced with H_2 at the same temperature (Fig. 8B). Initially, H_2 is completely consumed and the evolution of N_2 is immediately observed (2.09×10^{-4} mol/g_{cat}); in correspondence with H_2 breakthrough, small amounts of NH_3 are produced (0.14×10^{-4} mol/g_{cat}). Water is formed during reduction, while negligible amounts of other products (e.g. NO, NO_2 and N_2O) have been observed. These results are almost superimposed to those observed in the case of the single Pt–Ba/Al_2O_3 catalyst (compare Fig. 3B and Fig. 8B), but the amounts of ammonia observed in this case are much lower (0.14×10^{-4} vs. 0.57×10^{-4} mol/g_{cat}). This clearly indicates that most of NH_3 formed over the Pt–Ba/Al_2O_3 catalyst bed is adsorbed onto the Fe-ZSM-5 catalyst bed placed downstream.

3.2.5.2. Presence of CO_2 + H_2O. The same lean–rich cycles have been performed in the presence of CO_2 and H_2O in the fed, and the results are reported in Fig. 8C and D.

NO is fully up-taken upon admission to the reactor until breakthrough that is seen at 62 s, well before than in the absence of CO_2 and H_2O (at 212 s; compare Fig. 8A and C). The production of N_2 is apparent slightly before the NO_x breakthrough. The amounts of nitrogen produced (1.23×10^{-4} mol/g_{cat}) compare nicely with the amounts of NH_3 slipped from the single LNT catalyst bed (1.17×10^{-4} mol/g_{cat}).

The amounts of N_2 produced during the lean phase over the LNT/SCR dual bed are greater in the presence than in the absence of CO_2 and H_2O (1.23×10^{-4} vs. 0.49×10^{-4} mol/g_{cat}, compare Tables 3 and 2) because CO_2 favours the net production of ammonia during the rich phase for reasons already discussed. As a matter of fact, the total production of ammonia is estimated by summing up the N-species produced upon O_2 admission, the amounts of N_2 produced during the lean phase and the NH_3 slip during the rich phase, so that we obtain 1.24×10^{-4} mol/g_{cat} vs. 0.63×10^{-4} mol/g_{cat} in the presence and absence of CO_2 and H_2O, respectively (compare Tables 3 and 2).

It is worth noting that NH_3 oxidation upon O_2 admission is negligible over the LNT/SCR dual bed, whereas large amounts of ammonia were oxidised over LNT + SCR physical mixture, both in the presence and in the absence of CO_2 and H_2O for reasons already discussed (compare Fig. 8C vs. Fig. 6E and Fig. 8A vs. Fig. 6A).

The lower amounts of stored NO_x in the presence than in the absence of CO_2 and H_2O (2.72×10^{-4} vs. 4.23×10^{-4} mol/g_{cat}) are mainly related to the effect of CO_2 on the NO_x storage over the LNT catalyst. However, the difference between the amounts of removed NO_x in the presence and in the absence of CO_2 and H_2O is smaller (3.96×10^{-4} vs. 4.72×10^{-4} mol/g_{cat}). In fact, the presence of CO_2 increases the selectivity to NH_3 that is trapped onto the SCR catalyst, which in turn accounts for the increase in the amounts of lean N_2 (1.23×10^{-4} vs. 0.49×10^{-4} mol/g_{cat}). This leads to an increase in the amounts of removed NO_x and eventually compensates in part for the negative effect on the storage of NO_x.

We note also that in the presence of CO_2 and H_2O, the net production of ammonia (i.e. N_2 formed in the lean phase + N-species formed upon admission of oxygen + NH_3 slip) is lower over the LNT/SCR dual bed than over the LNT/SCR physical mixture (1.24×10^{-4} vs. 1.99×10^{-4} mol/g_{cat}); this confirms that over the LNT/SCR physical mixture during the reduction of stored NO_x, ammonia is preserved from further reaction to give nitrogen more effectively than over the LNT/SCR dual bed in the presence of CO_2 and H_2O as well.

Fig. 8C also shows that the oxidation of NO to NO_2 is strongly inhibited in the presence of H_2O over the LNT/SCR dual bed as well, since 58 ppm of NO_2 are formed at steady state vs. 344 ppm in the dry environment (Fig. 7A). The evolution of NO_2 is seen after the N_2 peak, due to the involvement of NO_2 in the fast SCR reaction or to the inhibition of ammonia on NO–NO_2 oxidation [29,33]. Alternatively, ammonia intercepts and reduces intermediate species in NO oxidation. Finally, small amounts of N_2 (associated to the oxidation of stored ammonia) are seen upon switch-on of the oxygen flow (0.013×10^{-4} mol/g_{cat}), due to the fact that desorbed NH_3 cannot be oxidised over the LNT catalyst, which is placed upstream.

The NO_x stored at 250 °C have been reduced with H_2 in the presence of CO_2 and H_2O at the same temperature (Fig. 7D). Only nitrogen is produced in appreciable quantities; few ppm of CO are also seen due to the RWGS reaction. The amounts of N_2 formed is lower in the presence than in the absence of CO_2 and H_2O (1.35×10^{-4} vs. 2.09×10^{-4} mol/g_{cat}), because of the lower amounts of stored NO_x (2.72×10^{-4} vs. 4.23×10^{-4} mol/g_{cat}). No ammonia slip is observed, while a small slip is detected in the absence of CO_2 and H_2O (0.14×10^{-4} mol/g_{cat}).

3.2.6. Effect of the temperature on the catalytic performances of the investigated systems

3.2.6.1. Absence of CO_2 + H_2O. Isothermal lean–rich cycles have been performed in the absence of CO_2 and H_2O over the single Pt–Ba/Al_2O_3 LNT catalyst, the LNT + SCR physical mixture and the LNT/SCR dual bed systems in the temperature range 150–350 °C. The results are displayed in terms of NO_x removed from the gas phase (Fig. 9), NH_3 slip (Fig. 10), N_2 production in the lean and rich phases (Fig. 11A–C) and ammonia oxidation upon oxygen admission (Fig. 7A in the case of LNT + SCR physical mixture).

Over the LNT catalyst, the amounts of NO_x removed increase with temperature (Fig. 9A) and show a maximum of 4.85×10^{-4} mol/g_{cat} at 300 °C, in line with previous literature reports [5,19,63]. The ammonia slip decreases with temperature (Fig. 10A) due to the higher relative importance of the reduction of nitrates by ammonia to give N_2 in the in series 2-steps reduction process for the reduction in stored NO_x [15–19]. N_2 is produced during the rich phase, with a maximum at 300 °C, but not during the lean phase (Fig. 11A). Finally, no oxidation of ammonia is observed upon oxygen admission as expected (not shown).

Over the LNT + SCR physical mixture, the amounts of NO_x removed (Fig. 9B) are higher than over the single LNT at $T \leqslant 250$ °C (Fig. 9A). The higher amounts of NO_x removed at low temperatures are due to the higher amounts of N_2 produced during the lean phase over the LNT + SCR physical mixture (Fig. 11B) due to the SCR reaction between gaseous NO_x, which slipped from the Pt–Ba/Al_2O_3 particles with NH_3 trapped onto the Fe-ZSM-5 particles (that are well mixed with the Pt–Ba/Al_2O_3 particles) during the previous rich phase. The amounts of trapped ammonia are higher at low temperatures considering that (i) the reduction of stored NO_x with hydrogen to give ammonia is faster than the reduction

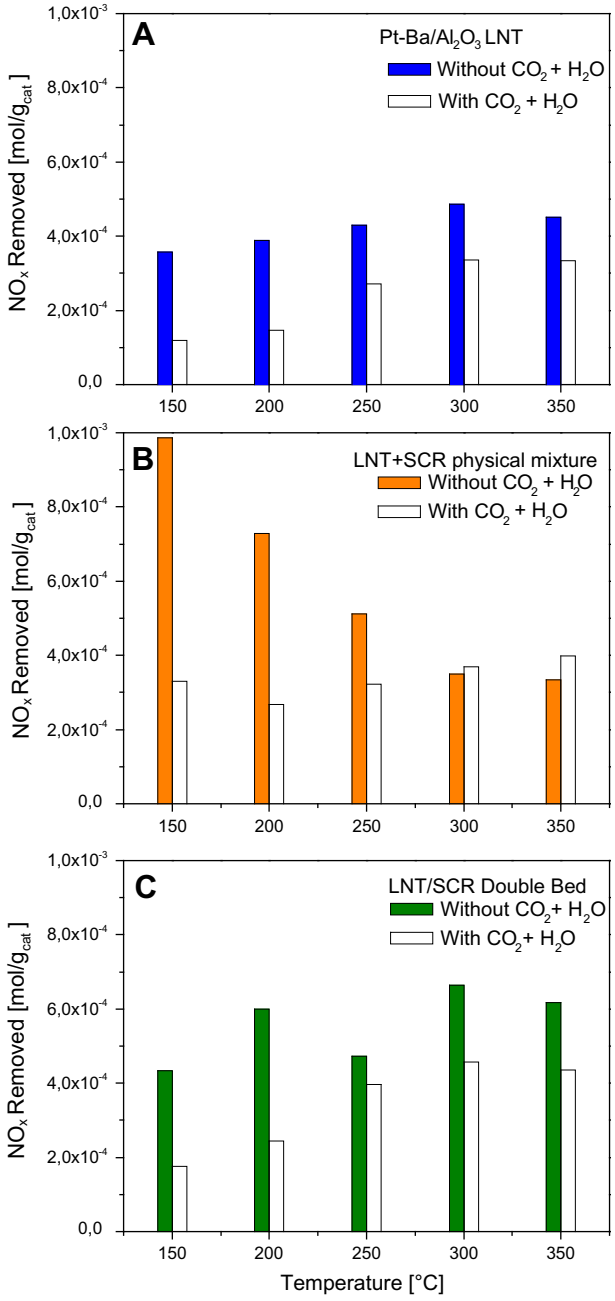

Fig. 9. Effect of the operative temperature on removed NO_x for (A) single LNT bed; (B) LNT + SCR physical mixture configuration; (C) LNT/SCR dual bed configuration. Filled coloured bar: absence of $CO_2 + H_2O$; unfilled bar: presence of CO_2 (0.3% v/v) + H_2O (1% v/v). Other experimental conditions as in Figs. 3, 6 and 8.

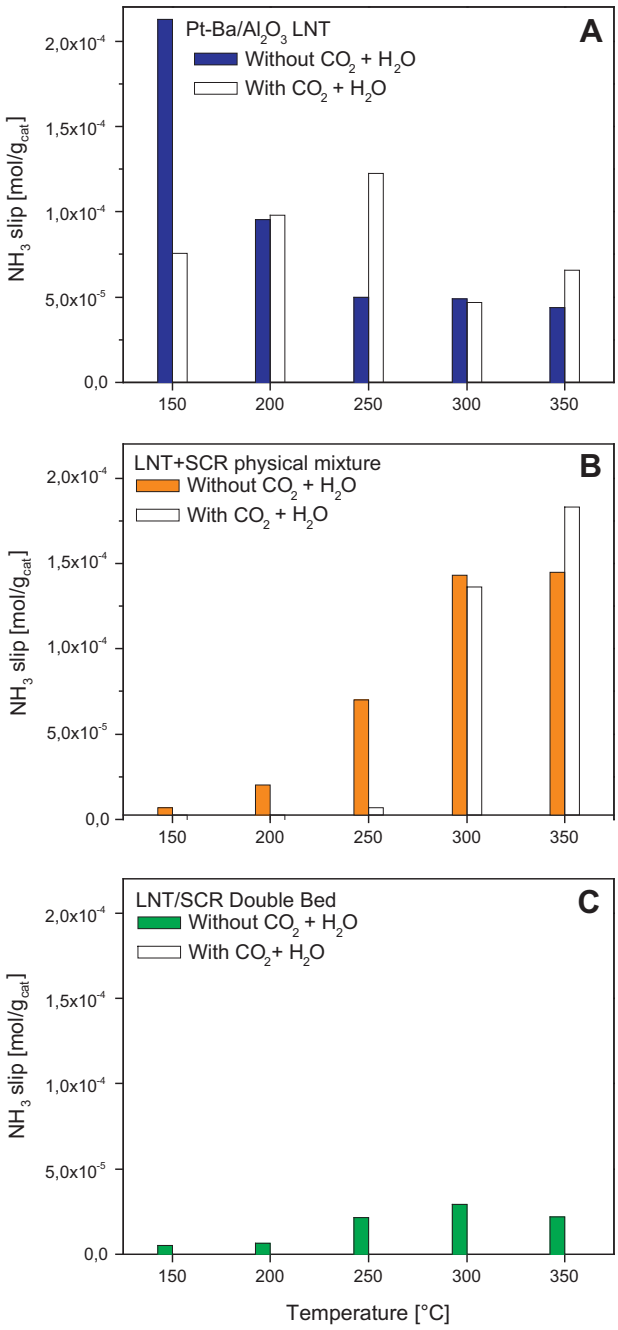

Fig. 10. Effect of the operative temperature on NH_3 slip for (A) single LNT bed; (B) LNT/SCR physical mixture configuration; (C) LNT/SCR dual bed configuration. Filled coloured bar: absence of $CO_2 + H_2O$; unfilled bar: presence of CO_2 (0.3% v/v) + H_2O (1% v/v). Other experimental conditions as in Figs. 3, 6 and 8.

of NO_x with ammonia to give nitrogen [17–19], and (ii) the adsorption of ammonia onto the Fe-ZSM-5 particles is favoured at low temperature. In view of this, the amounts of N_2 produced during the lean phase are high at low temperature but decrease with temperature (Fig. 11B). However, it is noted that from 250 °C, a large amount of stored ammonia is oxidised immediately upon oxygen admission (Fig. 7A) and this explain the marked drop in the amounts of N_2 formed during the lean phase at this temperature in Fig. 11B. The oxidation of ammonia upon oxygen admission is negligible below 250 °C. Still the amounts of N_2 formed during the lean phase plus the amounts of ammonia oxidised upon oxygen admission decrease with temperature from 2.2×10^{-4} mol/g_{cat} at 250 °C to 0.48×10^{-4} mol/g_{cat} at 350 °C because both the formation of ammonia and the adsorption of ammonia, which is the intermediate in the 2-steps reduction process of stored NO_x, are less favoured with temperature. For the same reasons, the amounts of N_2 formed during the rich phase increase with temperature (Fig. 11B).

It is also apparent in Fig. 10B that the ammonia slip over the LNT + SCR physical mixture is small (almost negligible) at low temperatures, increases with temperature and at $T \geqslant 250$ °C is higher than over the single LNT (compare Fig. 10B with Fig. 10A). The increase in the ammonia slip with temperature is due to the fact that the adsorption of ammonia onto the SCR catalyst particles is less favoured at high temperature: this leads to a 'chromatographic' effect on the NH_3 evolution caused by the presence of the zeolite

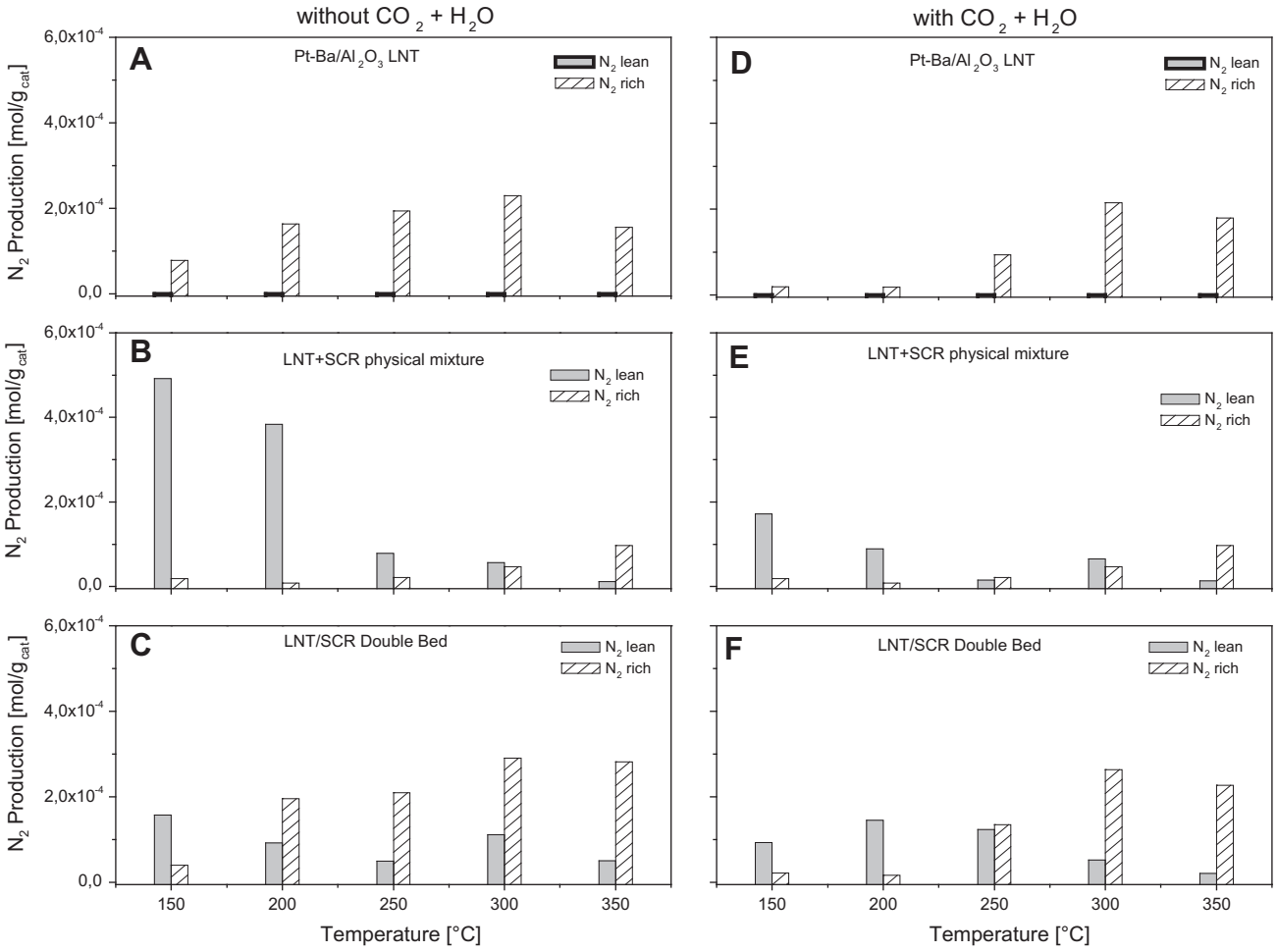

Fig. 11. Effect of the operative temperature on N_2 production in the absence of $CO_2 + H_2O$: (A) single LNT bed; (B) LNT + SCR physical mixture configuration; C) LNT/SCR dual bed configuration; in the presence of CO_2 (0.3% v/v) + H_2O (1% v/v): (D) single LNT bed; (E) LNT + SCR physical mixture configuration; (F) LNT/SCR dual bed configuration. Unfilled bar: N_2 lean production, filled bar: N_2 rich production. Other experimental conditions as in Figs. 3, 6 and 8.

catalyst particles. In fact, in line with the proposed pathway for nitrate reduction and due to the integral behaviour of the reactor, an H_2 front develops, which travels along the reactor during LNT regeneration [19,38]. NH_3 that is formed in the first step of the reduction process over the LNT particles (reaction (4)) is trapped on the zeolite catalyst particles that are well mixed within the LNT + SCR physical mixture, and this prevents NH_3 to react with nitrates stored on the LNT particles downstream to give N_2 (reaction (5)). The trapping is very efficient at low temperature, and this preserves NH_3 which in fact reacts with NO during the subsequent lean phase (large amounts of N_2 are produced during the lean phase, see Fig. 11B). At high temperature, the trapping onto the zeolite is less efficient and NH_3 is adsorbed but more easily desorbed from the zeolite particles. As a result, ammonia evolution is delayed while travelling along the reactor (chromatographic effect) and this prevents ammonia to react with nitrates stored onto the LNT particles downstream, because these nitrate species have already been reduced by H_2. Hence, a significant slip of ammonia is observed in this case, higher than over the single LNT catalyst bed (Fig. 10B vs. Fig. 10A).

Over the LNT/SCR dual bed, the amounts of removed NO_x are higher than over the single LNT catalyst at any temperature (Fig. 9C vs. Fig. 9A). Indeed, the amounts of NO_x removed over the LNT/SCR dual bed originate from the storage of NO_x over the LNT bed (Fig. 9A) and from the production of N_2 during the lean phase over the SCR bed (Fig. 11C). This last contribution is due to the SCR reactions between gaseous NO_x slipped from the LNT bed with ammonia stored onto the zeolite bed located downstream. The N_2 production during the lean phase decreases with temperature except at 300 °C (Fig. 11C) due to the decrease in the ammonia slipped during the rich phase from the single LNT catalyst and stored over the SCR downstream (Fig. 10A). The higher relative importance with temperature of the nitrate reduction by ammonia in the in series 2-steps reduction pathway of the reduction of stored NO_x also accounts for the increase with temperature of N_2 production during the rich phase (Fig. 11C). The ammonia slip over the LNT/SCR dual bed (Fig. 10C) is low at any temperature due to the presence of the SCR bed downstream of the LNT bed and of the fact that the adsorption of ammonia is favoured at low temperature [19] where the net formation of ammonia over the LNT catalyst is higher [15–19].

3.2.6.2. Presence of $CO_2 + H_2O$. Figs. 9, 10, 11D–F and Fig. 7B show also the results of isothermal lean–rich cycles performed in the presence of CO_2 and H_2O over the single Pt–Ba/Al_2O_3 LNT catalyst, the LNT + SCR physical mixture and LNT + SCR dual bed systems in the temperature range 150–350 °C.

In the case of the single LNT catalyst in the entire temperature range, the amounts of NO_x removed are lower in the presence than in the absence of CO_2 and H_2O (Fig. 9A) due to the inhibition of CO_2 on the storage of NO_x. The ammonia slip is lower at 150 °C (Fig. 10A) but is comparable at high temperature.

In the case of the physical mixture, the presence of CO_2 and H_2O causes a marked drop in NO_x removal (Fig. 9B) and in the amounts of N_2 formed during the lean phase (Fig. 11E) at $T \leqslant 250$ °C due to the inhibiting effect of CO_2 on the NO_x storage. Starting from 250 °C, a significant oxidation of ammonia stored onto the Fe-ZSM-5 particles during the rich phase of the previous cycle is observed upon oxygen admission (Fig. 7B). The extent of ammonia oxidation is greater and the selectivity to nitrogen is higher in the presence than in the absence of CO_2 and H_2O. For example, at 250 °C, the amounts of ammonia oxidised are 1.77×10^{-4} mol/g_{cat} and the selectivity to nitrogen is almost complete in the presence of CO_2 and H_2O, while in the absence 1.42×10^{-4} mol/g_{cat} of ammonia are oxidised and the selectivity to nitrogen is 54% (78% at 300 °C and 97% at 350 °C). As previously discussed, this behaviour is specific of the LNT + SCR physical mixture and is associated with the desorption of ammonia from the Fe-ZSM-5 particles and the effective contact between the particles of the SCR component and of the LNT component where ammonia is oxidised. The desorption of ammonia from the zeolite particles is favoured in the presence of water although to a very limited extent but the effect is amplified by the consecutive oxidation of ammonia. The oxidation of ammonia is more selective to nitrogen at high temperature: this behaviour is not fully understood at present and deserves further investigation.

The amounts of ammonia slip (Fig. 10B) are negligible at low temperatures and increase with temperature. This is primarily related with the reduction of NO_x stored over the LNT catalyst with ammonia as intermediate and with the arrangement of the LNT + SCR hybrid system characterised by the extensive contact between the Pt–Ba/Al_2O_3 and Fe-ZSM-5 particles. Indeed, at low *T*, the reduction of stored NO_x to give ammonia is more favoured as compared to the consecutive reduction of residual nitrates to give N_2 [17–19] while the adsorption of ammonia over the SCR catalyst is more favoured at low *T*. In the presence of H_2O and CO_2 at low temperature, the amounts of stored NO_x, which are reduced with hydrogen are lower [17–19], so that the amounts of ammonia produced by the reduction are smaller and the amounts of ammonia slip are smaller as well than in the absence of CO_2 and H_2O. At $T \geqslant 300$ °C, the NH_3 slip is comparable to those measured in the absence of CO_2 and H_2O.

In the case of the LNT/SCR dual bed, again the amounts of NO_x removed are lower at any temperature (Fig. 9C) because of the inhibition of CO_2 on the storage of NO_x. Besides, the amounts of N_2 formed during the lean phase tend to decrease with temperature (Fig. 11F) except at 150 °C, because the nitrate reduction by ammonia to give N_2 is favoured and accordingly the amounts of ammonia slipped from the LNT bed are smaller. The ammonia slip is negligible at any temperature and is lower in the presence than in the absence of CO_2 and H_2O for reasons already discussed (Fig. 9C).

4. Conclusive remarks

In the present paper, the performances of Pt–Ba/Al_2O_3 and Fe-ZSM-5 and of different hybrid Pt–Ba/Al_2O_3 + Fe-ZSM-5 systems where the LNT catalyst bed is placed in front of the SCR catalyst bed and the LNT and the SCR catalyst particles are physically mixed have been systematically investigated in the storage-reduction of NO_x. The study has been accomplished using small concentration of H_2, in the presence and absence of CO_2 and H_2O and in a wide temperature interval (150–350 °C) in order to operate under nearly isothermal conditions and to address the effect of CO_2 and H_2O and of temperature. The combined use of ISC experiments and FTIR spectroscopy has allowed following the storage-reduction of NO_x both in the gas phase and at the catalyst surface. The results have been explained at the quantitative level using the 2-steps pathway of the reduction of stored NO_x to give nitrogen with ammonia as intermediate, which was recently identified for the regeneration of LNTs and considering the integral behaviour of the reactor.

The following main points have been clarified:

(1) The storage of NO_x occurs primarily onto Pt–Ba/Al_2O_3, although a small contribution of Fe-ZSM-5 is possible and results in the formation of nitrate species, well recognised by FTIR over both Pt–Ba/Al_2O_3 and Fe-ZSM-5 at the end of the storage phase. In the presence of CO_2 and H_2O, the storage of NO_x is lower because $BaCO_3$ is formed, which retards NO_x adsorption.

(2) NH_3 formed as intermediate in the nitrate reduction to give N_2 over Pt–Ba/Al_2O_3 is trapped onto the Fe-ZSM-5 catalyst. The trapping of NH_3 is most favoured at low temperature and when the particles of Pt–Ba/Al_2O_3 and of Fe-ZSM-5 are evenly distributed in the reactor, as in the case of the LNT + SCR physical mixture. Indeed, trapping of NH_3 onto the Fe-ZSM-5 particles prevents the reaction of NH_3 with NO_x stored downstream onto Pt–Ba/Al_2O_3 particles to give N_2. NH_3 trapped onto Fe-ZSM-5 during the rich phase reacts during the subsequent lean phase with gaseous NO_x slipped from the Pt–Ba/Al_2O_3 to give N_2 according to standard SCR reaction.

(3) The NO_x removal efficiency is always higher for the hybrid LNT–SCR systems, both dual bed and physical mixture compared to single LNT, in the absence and in the presence of CO_2 and H_2O. This is due to the contribution of NO_x stored onto the LNT catalyst and of N_2 produced by the SCR reactions over the Fe-ZSM-5 catalyst during the lean phase. Note that the presence of CO_2 and H_2O reduces the NO_x removal efficiency over all the investigated systems.

(4) In the case of the LNT + SCR physical mixture, NH_3 trapped onto the Fe-ZSM-5 particles can be oxidised over the LNT particles immediately upon admission of oxygen to give N_2, N_2O and NO. The selectivity to nitrogen is almost complete in the presence of CO_2 and H_2O at any temperature.

(5) The ammonia slip is low to the best over the LNT/SCR dual bed at all investigated temperatures in the absence of CO_2 and H_2O. In the presence of CO_2 and H_2O, the ammonia slip is nil at any temperature over the LNT/SCR dual bed.

It is noted that the successful quantitative analysis of the data developed in the present study by using the 2-steps in series process of the reduction of stored NO_x by hydrogen further supports this scheme of regeneration of LNTs under nearly isothermal conditions and can be exploited to lower the PMG usage.

References

[1] A. Güthenke, D. Chatterjee, M. Weibel, B. Krutzsch, P. Kočí, M. Marek, I. Nova, E. Tronconi, Avd. Chem. Eng. 33 (2008) 103.
[2] P. Forzatti, Appl. Catal. A: Gen. 222 (2001) 221.
[3] L. Lietti, G. Ramis, F. Berti, G. Toledo, R. Robba, G. Busca, P. Forzatti, Catal. Today 42 (1998) 101.
[4] N. Takahashi, H. Shinjoh, T. Iijima, T. Suzuki, K. Yamazaki, K. Yokota, H. Suzuki, N. Niyoshi, S. Matsumoto, S. Tanizawa, S. Tanaka, T. Tateishi, K. Kashara, Catal. Today 27 (1996) 63.
[5] W.S. Epling, L.E. Campbell, A. Yezerets, N.W. Currier, J.E. Parks, Catal. Rev. Sci. Eng. 46 (2004) 163.
[6] S. Matsumoto, Catal. Today 90 (2004) 183.
[7] T. Johnson, Platinum Metals Rev. 52 (2008) 23.
[8] C. Enderle, G. Vent, M. Paule, SAE Technical Paper 2008-01-1182.
[9] S. Bremm, M. Pfeifer, J. Lepre, W. Mueller, S. Kurze, M. Paule, B. Keppeler, G. Vent, SAE Tecnical Paper 2008-01-1184.
[10] A. Kato, S. Matsuda, T. Kamo, F. Nakajima, H. Kuroda, T. Narita, J. Phys. Chem. 85 (1981) 4099.
[11] M. Koebel, M. Elsener, G. Madia, Ind. Eng. Chem. Res. 40 (2001) 52.
[12] P. Forzatti, I. Nova, E. Tronconi, Angew. Chem. Int. Edit. 48 (2009) 8366.

[13] P. Forzatti, I. Nova, E. Tronconi, Ind. Eng. Chem. Res. 49 (2010) 10386.
[14] L. Lietti, P. Forzatti, F. Bregani, Ind. Eng. Chem. Res. 35 (1996) 3384.
[15] I. Nova, L. Castoldi, L. Lietti, E. Tronconi, P. Forzatti, F. Prinetto, G. Ghiotti, J. Catal. 222 (2004) 377.
[16] F. Prinetto, G. Ghiotti, I. Nova, L. Castoldi, L. Lietti, E. Tronconi, P. Forzatti, Phys. Chem. Chem. Phys. 5 (2003) 4428.
[17] P. Forzatti, L. Lietti, I. Nova, Energy Environ. Sci. 1 (2008) 236.
[18] I. Nova, L. Lietti, P. Forzatti, Catal. Today 136 (2008) 128.
[19] L. Lietti, I. Nova, P. Forzatti, J. Catal. 257 (2008) 270.
[20] L. Castoldi, L. Lietti, P. Forzatti, S. Morandi, G. Ghiotti, F. Vindigni, J. Catal. 276 (2010) 335.
[21] L. Cumaranatunge, S.S. Mulla, A. Yezerets, N.W. Currier, W.N. Delgass, F.H. Ribeiro, J. Catal. 246 (2007) 29.
[22] J.A. Pihl, J.E. Parks II, C.S. Daw, T.W. Root, SAE Technical Paper, 2006-01-3441
[23] M. Weibel, N. Waldbüßer, R. Wunsch, D. Chatterjee, B. Bandl-Konrad, B. Krutzsch, Top. Catal. 52 (2009) 1702.
[24] J. Theis, E. Gulari, SAE Technical Paper, 2006-01-0210.
[25] R. Snow, D. Dobson, R. Hammerle, S. Katare, SAE Technical Paper, 2007-01-0469.
[26] J. McCarthy Jr., T. Korhumel Jr., A. Marougy, SAE Int. J. Commer. Veh. 2 (2010) 34.
[27] L. Xu, R. McCabe, W. Ruona, G. Cavataio, SAE Technical Paper, 2009-01-0285.
[28] J. Parks, V. Prikhodko, SAE Technical Paper, 2009-01-2739.
[29] P. Forzatti, L. Lietti, Catal. Today 155 (2010) 131.
[30] E.C. Corbos, M. Haneda, X. Courtois, P. Marecot, D. Duprez, H. Hamada, Catal. Commun. 10 (2008) 137.
[31] E.C. Corbos, M. Haneda, X. Courtois, P. Marecot, D. Duprez, H. Hamada, Appl. Catal. A: Gen. 365 (2009) 187.
[32] A. Lindholm, H. Sjövall, L. Olsson, Appl. Catal. B: Environ. 98 (2010) 112.
[33] R. Bonzi, L. Lietti, L. Castoldi, P. Forzatti, Catal. Today 151 (2010) 376.
[34] N. Miyoshi, T. Tanizawa, K. Kasahara, S. Tateishi, European Patent Application 0 669 157 A1, 1995.
[35] I. Nova, L. Castoldi, F. Prinetto, V. Dal Santo, L. Lietti, E. Tronconi, P. Forzatti, G. Ghiotti, R. Psaro, S. Recchia, Top. Catal. 30/31 (2004) 181.
[36] L. Castoldi, I. Nova, L. Lietti, P. Forzatti, Catal. Today 96 (2004) 43.
[37] I. Nova, L. Castoldi, L. Lietti, E. Tronconi, P. Forzatti, F. Prinetto, G. Ghiotti, SAE Technical Paper, 2005-01-1085.
[38] P. Forzatti, L. Lietti, N. Gabrielli, Appl. Catal. B: Environ. 99 (2010) 145.
[39] F. Prinetto, G. Ghiotti, I. Nova, L. Lietti, E. Tronconi, P. Forzatti, J. Phys. Chem. C 105 (2001) 12732.
[40] F. Frola, M. Manzoli, F. Prinetto, G. Ghiotti, L. Castoldi, L. Lietti, J. Phys. Chem. C 112 (2008) 12869.
[41] M.M.J. Treacy, J.B. Higgins (Eds.), Collection of simulated XRD powder patterns for zeolites, fourth revised ed., Elsevier, 2001.
[42] M.S. Kumar, M. Schwidder, W. Gruenert, A. Brueckner, J. Catal. 227 (2004) 384.
[43] A.M. Ferretti, A.-L. Barra, L. Forni, C. Oliva, A. Schweiger, A. Ponti, J. Phys. Chem. B 108 (2004) 1999.
[44] A. Brueckner, R. Lück, W. Wieker, B. Fahlke, H. Mehner, Zeolites 12 (1992) 380.
[45] D. Goldfarb, M. Bernardo, K.G. Strohmaier, D.E.W. Vaughan, H. Thomann, J. Am. Chem. Soc. 116 (1994) 6344.
[46] P. Wenquin, O. Shilun, K. Zhiyun, P. Shaoyi, Stud. Surf. Sci. Catal. 49 (1989) 218.
[47] A.F. Ojo, J. Dwyer, R.V. Parish, Stud. Surf. Sci. Catal. 49 (1989) 227.
[48] E.A. Zhilinskaya, G. Delahay, M. Mauvezin, B. Coq, A. Aboukais, Langmuir 19 (2003) 3596.
[49] A.A. Aboukais, E.A. Zhilinskaya, I.N. Filimonov, N.S. Nesterenko, S.E. Timoshin, I.I. Ivanova, Catal. Lett. 111 (2006) 97.
[50] B. Wichterlova, L. Kubelkova, P. Jiru, D. Kolihova, Collect. Czech. Chem. Commun. 45 (1980) 2143.
[51] S. Bordiga, R. Buzzoni, F. Geobaldo, C. Lamberti, E. Giamello, A. Zecchina, G. Leofanti, G. Petrini, G. Tozzola, G. Vlaic, J. Catal. 158 (1996) 486.
[52] H.H. Tippins, Phys. Rev. B 72 (1970) 279.
[53] P. Wu, T. Komatsu, T. Yashima, Micropor. Mesopor. Mater. 20 (1998) 139.
[54] L. Capek, V. Kreibich, J. Dedecek, T. Grygar, B. Wichterlova, Z. Sobalik, J.A. Martens, R. Brosius, V. Tokarova, Micropor. Mesopor. Mater. 80 (2005) 279.
[55] M. Schwidder, S. Heikens, A. De Toni, S. Geisler, M. Berndt, A. Brückner, W. Grünert, J. Catal. 259 (2008) 96.
[56] P. Balle, B. Geiger, S. Kureti, Appl. Catal. B 85 (2008) 109.
[57] J. Perez-Ramirez, J.C. Groen, A. Brückner, M.S. Kumar, U. Bentrup, M.N. Debbagh, L.A. Villaescusa, J. Catal. 232 (2005) 318.
[58] M. Ahrens, O. Marie, P. Bazin, M. Daturi, J. Catal. 271 (2010) 1.
[59] G.W. Graham, H.-W. Jen, O. Ezekoye, R.J. Kudla, W. Chun, X.Q. Pan, R.W. McCabe, Catal. Lett. 116 (2007) 1–8.
[60] F. Frola, F. Prinetto, G. Ghiotti, L. Castoldi, I. Nova, L. Lietti, P. Forzatti, Catal. Today 126 (2007) 81.
[61] A. Lindholm, N.W. Currier, E. Fridell, A. Yezerets, L. Olsson, Appl. Catal. B Environ. 75 (2007) 78.
[62] L. Olsson, M. Abul-Milh, H. Karlsson, E. Jobson, P. Thormaehlen, A. Hinz, Top. Catal. 30/31 (2004) 85.
[63] S.S. Mulla, N. Chen, L. Cumaranatunge, W.N. Delgass, W.S. Epling, F.H. Ribeiro, Catal. Today 114 (2006) 57.
[64] F. Frola, Ph.D. Thesis, University of Turin, 2007.
[65] M. Rivallan, G. Ricchiardi, S. Bordiga, A. Zecchina, J. Catal. 264 (2009) 104.
[66] A. Grossale, I. Nova, E. Tronconi, Catal. Today 136 (2008) 18.
[67] S. Brandenberger, O. Kröcher, A. Tissler, R. Althoff, Catal. Rev. 50 (2008) 492.
[68] M.S. Kumar, M. Schwidder, W. Grünert, U. Bentrup, A. Brückner, J. Catal. 239 (2006) 173.
[69] Y.H. Yeom, B. Wen, W.M.H. Sachtler, E. Weitz, J. Phys. Chem. B 108 (2004) 5386.
[70] Y.H. Yeom, J. Henao, M.J. Li, W.M.H. Sachtler, E. Weitz, J. Catal. 231 (2005) 181.
[71] O. Kröcher, M. Devadas, M. Elsener, A. Wokaun, N. Söger, M. Pfeifer, Y. Demel, L. Mussmann, Appl. Catal. B: Environ. 66 (2006) 208.
[72] E. Tronconi, I. Nova, C. Ciardelli, D. Chatterjee, B. Bandl-Konrad, T. Burkhardt, Catal. Today 105 (2005) 529.
[73] M. Devadas, O. Kröcher, M. Elsener, A. Wokaun, G. Mitrikas, N. Söger, M. Pfeifer, Y. Demel, L. Mussmann, Catal. Today 119 (2007) 137.
[74] C. Ciardelli, I. Nova, E. Tronconi, B. Bandl-Konrad, D. Chatterjee, M. Weibel, B. Krutzsch, Appl. Catal. B: Environ. 70 (2007) 80.
[75] A. Grossale, I. Nova, E. Tronconi, D. Chatterjee, M. Weibel, J. Catal. 256 (2008) 312.
[76] F. Yin, A.L. Blumenfeld, V. Gruver, J.J. Fripiat, J. Phys. Chem. B 101 (1997) 1824.
[77] S. Bodoardo, R. Chiappetta, B. Onida, F. Figueras, E. Garrone, Macropor. Mesopor. Mater. 20 (1998) 187.
[78] E. Tronconi, L. Lietti, P. Forzatti, S. Malloggi, Chem. Eng. Sci. 51 (1996) 2965.
[79] L. Lietti, I. Nova, S. Camurri, E. Tronconi, P. Forzatti, AIChE J. 43 (1997) 2559.